A Transparent, Compliant, Model of the Inferior Vena Cava for Haemodynamic Analysis in Right Heart Simulator.

Ciara Dillon

School of Mechanical and Materials Engineering

MEEN30180 Professional Engineering Project (Mechanical)

Supervisor: Dr Malachy O'Rourke

24th April 2023

UCD School of Mechanical and Materials Engineering

Report Submission Form

This form should be completed and signed. It should be incorporated into your submission (PDF and hard copy versions) and should appear as a single page immediately after the title page.

Student Name: Ciara Dillon

Student Number: 19370253

Report Title: Investigation of the IVC and developing phantom of high bio-fidelity showing the mechanical characterization and

Plagiarism

Plagiarism is a serious academic offence and is comprehensively dealt with on UCD's Registry website (https://www.ucd.ie/governance/resources/policypage-plagiarismpolicy). It is a student's responsibility to be familiar with the University's policy on plagiarism. All students are encouraged, if in doubt, to seek guidance from an academic member of staff on this issue. The UCD policy document on plagiarism states that "the University understands plagiarism to be the inclusion of another person's writings or ideas or works, in any formally presented work (including essays, theses, projects, laboratory reports, examinations, oral, poster or slide presentations) which form part of the assessment requirements for a module or programme of study, without due acknowledgement either wholly or in part of the original source of the material through appropriate citation. Plagiarism is a form of academic dishonesty, where ideas are presented falsely, either implicitly or explicitly, as being the original work of the author. While plagiarism may be easy to commit unintentionally, it is defined by the act not the intention. The University advocates a developmental approach to plagiarism and encourages students to adopt good academic practice by maintaining academic integrity in the presentation of all academic work".

Declaration of Authorship

I declare that all material in this submission is my own work except where there is clear acknowledgement and appropriate reference to the work of others.

Signature: Ciara Dillon Date: 21/04/2023

ABSTRACT:

Cardiovascular simulated systems allow for the analysis and understanding of anatomy response and function. In this investigation, a phantom is created to mimic the Inferior Vena Cava's response to cardiovascular and respiratory cycles and to allow for Particle Image Velocimetry (PIV) analysis on the model. A model made from Sylgard-184 is successfully placed in the Right Heart Simulator along with preliminary PIV Analysis techniques. Sylgard-184 proves to be stiffer than the previous material used DragonSkin FX-Pro with a low strain elastic modulus of approximately 0.81 MPa from preliminary cyclical testing done.

PIV analysis is a non-invasive technique for flow visualization to gain further understanding of response to changes in pressures and flow velocity. A phantom of high optical clarity and compliance is required and the PDMS Elastomer, Sylgard-184 is used (Dow Corning). The design of the phantom is for the purpose of attachment to a water-pressurized chamber, in the right-heart simulator in UCD Mechanical Engineering Laboratory. Sylagrd-184 facilitates the study of the collapse of the IVC in relation to cardiovascular and respiratory cycles, using PIV Analysis.

The Inferior Vena Cava is part of the right-side cardiovascular system, it is noted that cardiovascular research is mainly focused on the left-side cardiovascular anatomies. Most literature to date is focused on IVC filters for pulmonary embolism and deep vein thrombosis prevention. Included in this study is the investigation into the viscoelastic properties of Sylgard-184 and how they relate to the biomechanical properties of the IVC venous tissue. Properties of compliance and hyper-viscoelasticity are further investigated.

ACKNOWLEDGEMENTS

I'd like to express my gratitude to my friends and family for their continuous encouragement during my time at UCD. Thank you for your patience and advice throughout this project.

I'd like to thank Dr. Malachy O'Rourke for his support during the project. Thank you for your patience, guidance, and encouragement throughout the year, and to the numerous master's students with whom I worked.

I'd like to thank everyone who helped me with this project, especially Wenting Shu, Kieran Gibbons, Ryan Paetzold, Derek O'Reilly, and Professor Eoin O'Cearbhaill. Thank you for your project feedback, comments, and advice; I learned a lot more than I expected from this project.

TABLE OF CONTENTS

LIST OF FIGURES

LIST OF TABLES

LIST OF EQUATIONS

NOMENCLATURE

IVC = Inferior Vena Cava

CVD = cardiovascular disease

ν = viscosity (Pa.s)

L = length of silicone tube (m)

r = radius of silicone tube (m)

Q = volumetric flow rate through the tube (m^3/s)

I = cross sectional area of moment of inertia per unit length

E = Young's Modulus

TEBV = Tissue Engineered Blood Vessels

TMM = Tissue Mimicking material

BMF = Blood Mimicking Fluid

1. Introduction

1.1 Background: Cardiovascular System and The Vena Cava

Cardiovascular diseases (CVDs) are of the leading causes of death worldwide. In 2019 an estimated 17.9 million people died from CVDs which is about 32% of all global deaths (WHO, 2021). To tackle this issue and develop more accessible and effective treatments for CVDs, studying the functions and responses of the cardiovascular systems is vital.

The cardiovascular system is continuously studied to gain further understanding of the mechanical properties of vascular tissues and the resulting hemodynamics from the stress response of these vessels combined with the cardiac and respiratory cycles. Simulated-use systems are developing worldwide allow for rapid prototyping and fast cycle iterations for medical devices and treatments for CVDs. Techniques such as ultrasound and optical imaging have been used to try to understand the mechanical response to disturbances in cardiovascular anatomies which results in possible compromise of circulation [11].

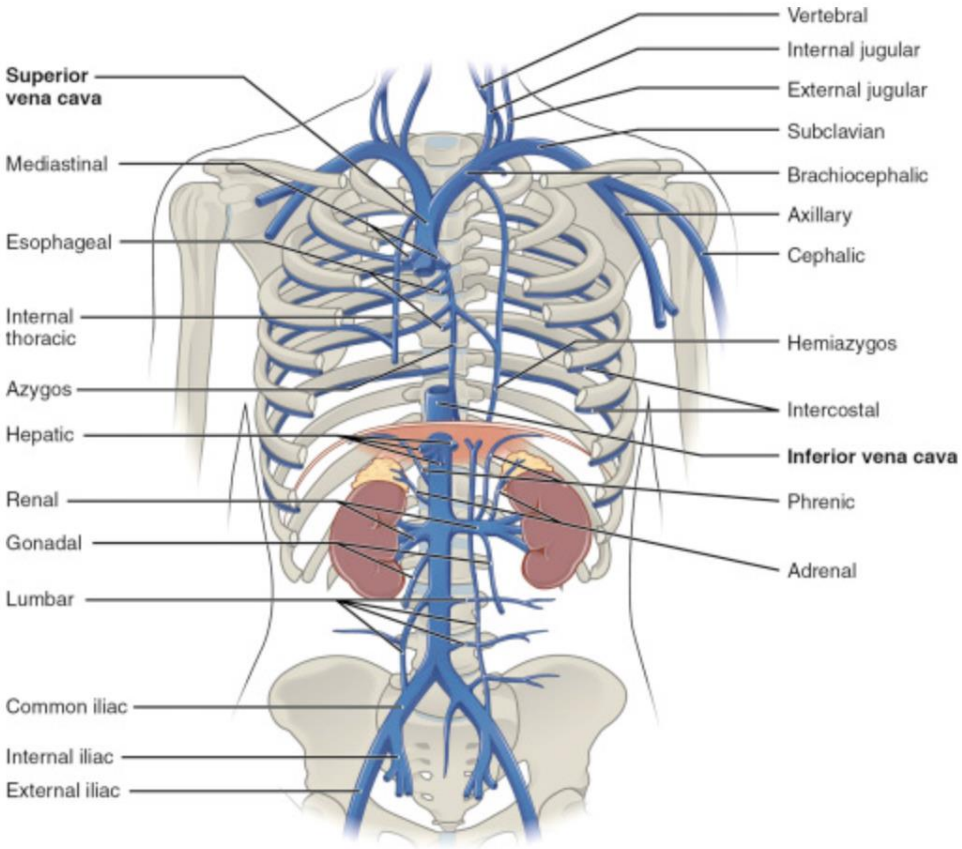

Figure 1: Inferior and Vena Cava segments attached to the right atrium [8]

The main challenge in replicating anatomy is the simulation of the complex soft cardiovascular tissue and its mechanical properties. In this study a phantom model of the Inferior Vena Cava will be produced to allow for blood-flow analysis of this vessel. A benchmark of porcine IVC tissue mechanical properties [12] will be used.

The Vena Cava is the largest blood vessel in the human body which returns deoxygenated blood back to the heart. It is split into the superior and inferior vena cava as shown in Figure 1. The superior vena cava returns blood from the upper extremities of the human body such as the arms and head whereas the inferior vena cava drains the blood from the lower extremities of the legs and the kidneys. The IVC is one of very few veins without valves and is one of the largest vessels in the human body [8].

1.2 Research Question and Project Aim

Invasive methods of surgically implanted flowmeters [13] and catheter-tip electromagnetic transducers[14] have been used to study the effects of cardiac and respiratory cycles on the blood flow through the IVC. PIV analysis provides a non-invasive method of analysis which can help one understand the velocity field within the IVC upon collapse.

Successful PIV analysis will provide an understanding into the response of the IVC to blood flows and pressures due to the respiratory and cardiac cycles that produce a biphasic flow and unique elliptical collapse corresponding to these cycles.

1.2.2 Overall Aims:

Improve the compliance of the IVC model to be placed in the Right Heart Simulator form the DragonSkin FXPro model produced from a previous master's student. This model should be less compliant, transparent for PIV analysis and be durable for attaching/detaching to the IVC water-pressurized chamber.

Analyze and investigate the properties of the material and the effect of curing temperature of the model on the viscoelastic properties. Provide a detailed description for the next steps of the project and further investigation into the tuning of Sylgard-184's mechanical properties.

1.3 Project Objectives

The main objective is to create a phantom that has the following requirements:

- Optically transparent with the refractive index matching the fluid (BMF) contained in the phantom and externally in the chamber.
- The geometry of the phantom must mimic the geometry of the IVC with high anatomical detail along with similar biomechanics properties such as compliance and viscoelasticity.
- Test Sylgard-184 for viscoelastic properties and compliance using a low-profile tensile tester and compliance rig.

1.4 Methodology

Dividing the two directions of this project into two separate components. One is for testing the changes in mechanical properties with the curing temperature of the Sylgard-184 which will be mentioned in 2.3.3.

1. Testing: Viscoelastic Properties and Strength

Using Lloyds LS 1 Series Materials Testing Machine – test rings of Sylgard-184 for viscoelastic properties and compare with previous material used Dragon Skin FX-Pro.

Investigatory pull-to-failure tests to be done on failed prototypes to understand the maximum axial strength that can be applied to a defective model.

2. Phantom Fabrication

Using 3D printed external moulds and aluminium mandrels, produce a phantom of high transparency for PIV Analysis for chamber. Several iterations of the phantom will be produced to improve the anatomical geometry, strength of the model and easier attachment of model to the chamber.

1.5 Thesis Layout

1.5.1 Introduction

Introduce the role of the inferior vena cava in the cardiovascular system along with the research question the project will be addressing, aims, objectives, methodologies, and report layout.

1.5.2 Literature Review

Thorough research into the functions of the Inferior Vena Cava, venous tissue biomechanics, hemodynamics of the IVC, alternative fabrication of phantoms, material properties of elastomers and more.

Topics include the cardiovascular system, anatomy of the Inferior Vena cava, hemodynamics, vascular biomechanics, compliance, methods of fabricating phantoms, alternative materials such as elastomers and finally testing techniques for materials that show viscoelastic behavior.

1.5.3 Methodology

Methods used throughout the project are described in detail for reproducibility and repeatability. These methods include the design of the model and samples produced, methods for injection moulding Sylagrd-184, the cyclical testing done on samples of the material and nonstandard testing done for further investigation to understand the limits of the material.

1.5.4 Results

Results from the modeling of the IVC are shown in this chapter, including the defective prototypes and observations from these failed models. The resulting final models are shown. Post-processed graphs are provided to show the effects of temperature on the viscoelastic properties of the material under strains below 40%.

1.5.5 Discussion

Summary of results including the prototyping stages, final models produced, PIV analysis, cyclical testing and investigatory testing done on defective models.

1.5.6 Conclusion

Conclusions drawn from experimental procedures, results from testing and further work that can be done. Limitations of the project are outlined and discussed along with reference to an appendix that includes drawings of the next possible design for the molds.

2. Literature Review

2.1 Cardiovascular Anatomy and Function

The cardiovascular system is composed of blood vessels, blood, and the heart. The main functions of the cardiovascular systems are the transport of molecules (oxygen, nutrient, carbon dioxide and metabolic waste products), defense/healing, thermoregulation and fluid balance [15]. The cardiovascular system contains a pulmonary and systemic circuit as shown in Figure 2. Blood is pumped by the heart, from the aorta to the arteries and the blood is returned to the heart by veins to the inferior and superior vena cava (systematic circuit).

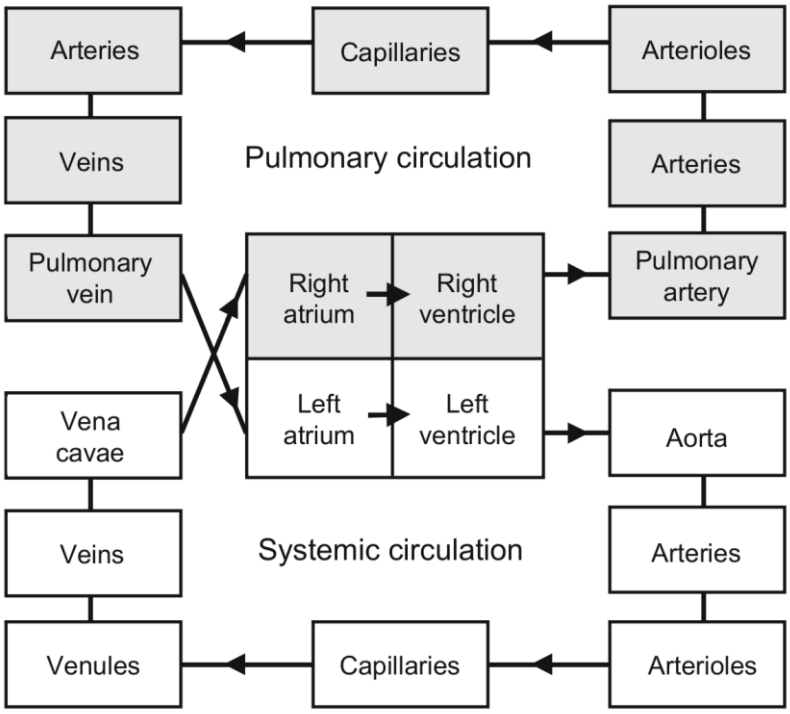

Figure 2: Components of the cardiovascular system showing the systemic circulatory in white and pulmonary circulation in grey. [15]

The venous system's function is to return deoxygenated blood to the heart, under low pressure conditions. Understanding venous biomechanics is important for understanding how the blood is returned to the heart and how external and internal environments affect this.

The systemic (greater) circulation involves the left ventricle pumping blood through the aorta through arteries, delivering oxygen and important molecules around the body, and back to the heart through veins and the vena cavae. The pulmonary circuit involves the circulation of blood from the heart to the lungs by the right and left pulmonary arteries. This circuit's primary function is the oxygenation of blood.

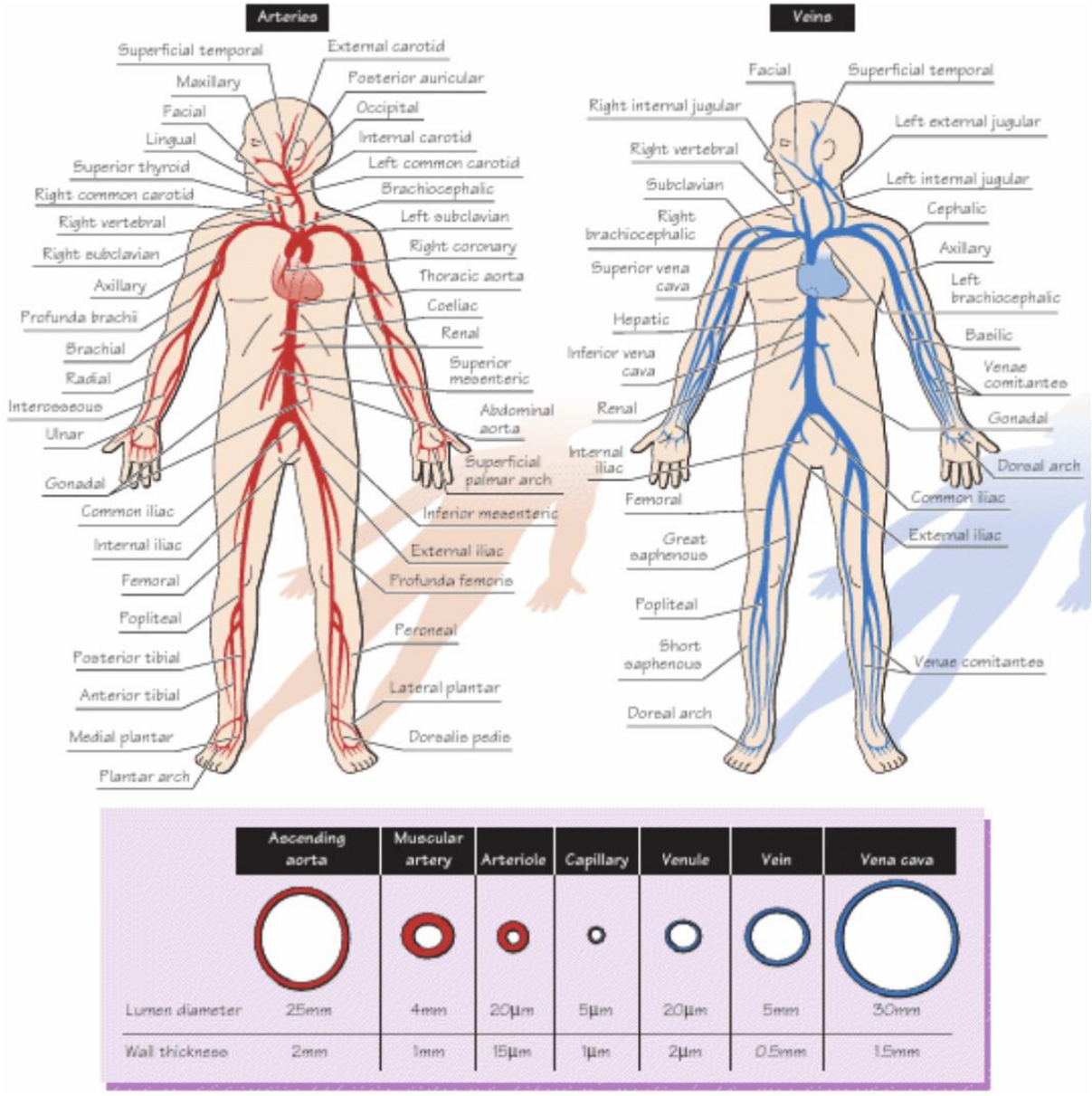

Figure 3: Comparison of arterial and venous cardiovascular anatomies with regards to location, lumen diameters and wall thickness. [4]

The blood vessels in the cardiovascular system act as a conduit for blood. Capillaries and venules act as exchange vessels as molecules are passed between their walls. Smaller arteries act as resistance as they regulate the amount of blood flowing to tissues through dilation and contraction [4] As shown in Figure 3 the arterial and venous systems have different characteristics with larger lumens for veins and thicker walls for arteries. This results in different pressures and flow rates in the vasculature.

2.2 The Venous System: The Inferior Vena Cava

The function of the venous system is to return deoxygenated blood to the right atrium through the Vena Cavae. Venules and veins have an important role of microcirculation and aid in the stabilization and regulation of the venous return to the heart. Comparing to the arterial system, the venous system holds approximately 60-80% of the total blood volume in the body [15]. This is due to:

1. A higher number of venules than arterioles in the venous system with larger internal lumen diameters
2. Thin-walled dimensions of veins allow for higher compliance and expansion as the internal pressure rises within the vessel. [4]

The storage capacity of the vena cavae depends on many factors which include geometry, material properties, influence of surrounding tissues and variation in transmural pressure.

$$Ptransmural = Pinternal - Pexternal \quad \textit{(Equation 1)}$$

Inferior Vena Cava

The inferior vena cava is a high compliant vessel which is reliant on ventilatory and circulatory cycles. It was shown that inspiration and expiration caused changing intrathoracic pressure resulting in the collapse of the Inferior Vena Cava [16]. The vessel returns blood from the lower body and its extremities. Its main tributaries include the hepatic veins, renal veins, and iliac veins.

Most of the literature done on the Inferior Vena Cava is done for IVC filter research for the treatment of venous thromboembolic disease. An IVC collapsibility index has been

developed to quantify the effect of breathing and alternative respiration methods on the collapse and distention of the vessel.

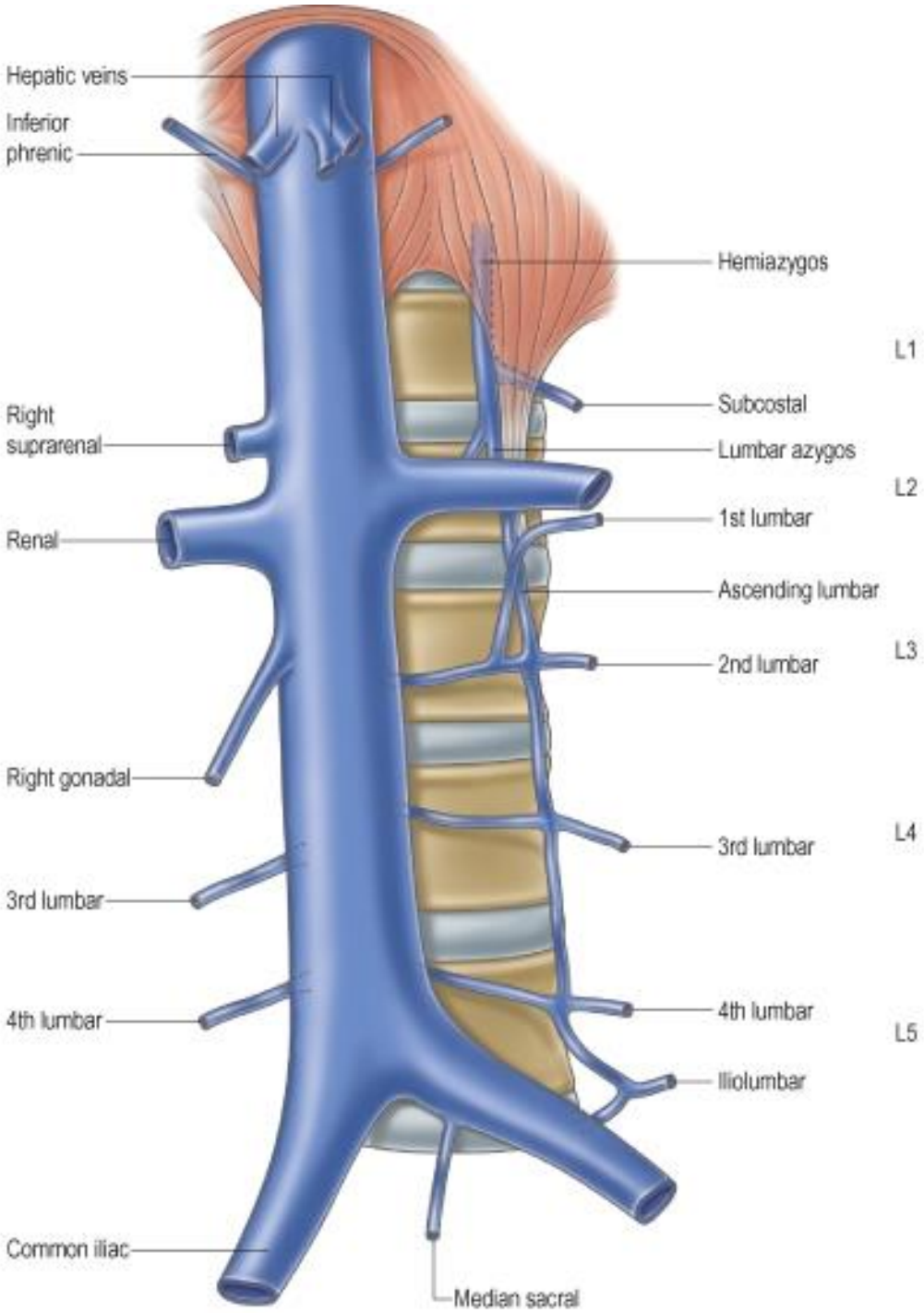

Figure 4: Inferior vena cava and its tributaries below the diaphragm (Source: Anatomy-medicine.com)

2.3 Vascular Biomechanics

Blood vessels are classified as soft tissue that does not obey Hooke's Law due to the non-linearity of their stress-strain relationship.

Fung claims that the most important feature of systematic veins is their compliance [1]. The venous system is known to be a 'flexible reservoir of blood' [8] which is vital for the "active" systemic blood. For example, throughout exercise, the percentage of blood in the venous system is reduced to almost 25% to allow for the majority of blood to be circulating in the arterial system through venous constriction.

2.3.1 Vessel Wall Composition

Vessels have three layers, the adventitia, media, and intima. Comparing venous and arterial compositions, the venous vessels have lower concentrations of smooth muscle and thinner walls. The adventitial layer is thicker than the medial layer and the elastic/collagen ratio is small compared to arteries. The composition of venous vessels results in stiffening when fully distended.

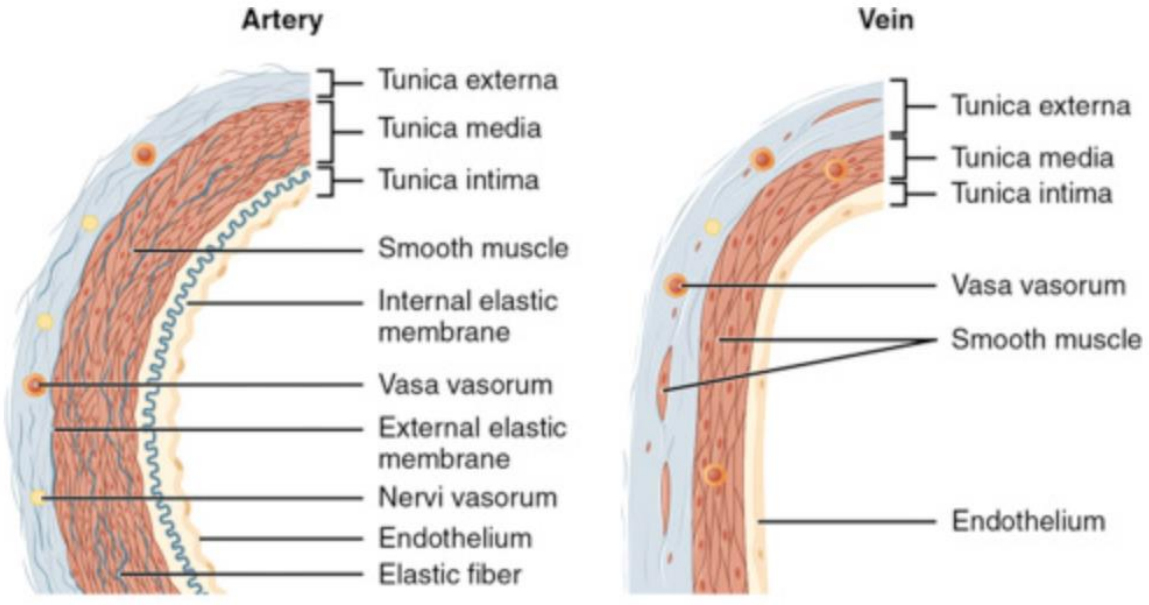

Figure 5: Comparison of thickness ratios of tunica extrema, media and intima for veins versus arteries [8]

2.3.2 Mechanical Properties of the IVC

The most important properties relating to the IVC are the compliance of the vessel and the dynamic tensile strength of the vessel which can be measured using a compliance testing fixture and uniaxial cyclical tensile testing.

The pressure within arteries and veins differs by approximately a factor of 10. The blood pressure in healthy veins is approximately 10 mmHg or less whereas in arteries it can reach 100 mmHg or more within the vessel. [8] The flow into the right atrium is also known as venous return and this is interdependent with cardiac output – a relation which is known as the Frank Starling Mechanism [17]. Rabbit IVC tissue was found to have an elastic modulus of 0.49 MPa in a study by Brown and Heistad (1985) [18] and 0.38 ± 0.51 MPa for porcine IVC tissue in the study by Snowhill and Silver (2013) [12].

Relating the IVC to a collapsible tube simplifies the mechanics of the vessel and allows us to simulate similar collapse *en vitro* to collapse of the IVC *en vivo*. [12]

2.3.3 Hyper-Viscoelasticity and Compliance

Cardiovascular tissues have been shown to demonstrate viscoelastic properties, which implies they have features of elastic and viscous solids. When determining the mechanical properties of this tissue, the dynamics of the tissue deformation is very important [19].

Compliance, which is also known as capacity, is defined as the change in volume/diameter for a given change in pressure. This can be compared to distensibility which is the fractional change in area to the given change in pressure. In the Wind Kessel Concept, the compliance component is treated as a capacitor. A vessel's stiffness can determine how compliant the vessel will be. The percentage of elastin to collagen is very important for distensibility. Elastin is easier to stretch compared to collagen and increases the flexibility of the vessel. Collagen increases the overall resistance to stresses [20].

Elastic instability causes the collapsibility of a vein when negative transmural pressure occurs intravascularly. An elliptical shape when a buckling pressure is reached in collapsible tubes as shown by Fung [1].

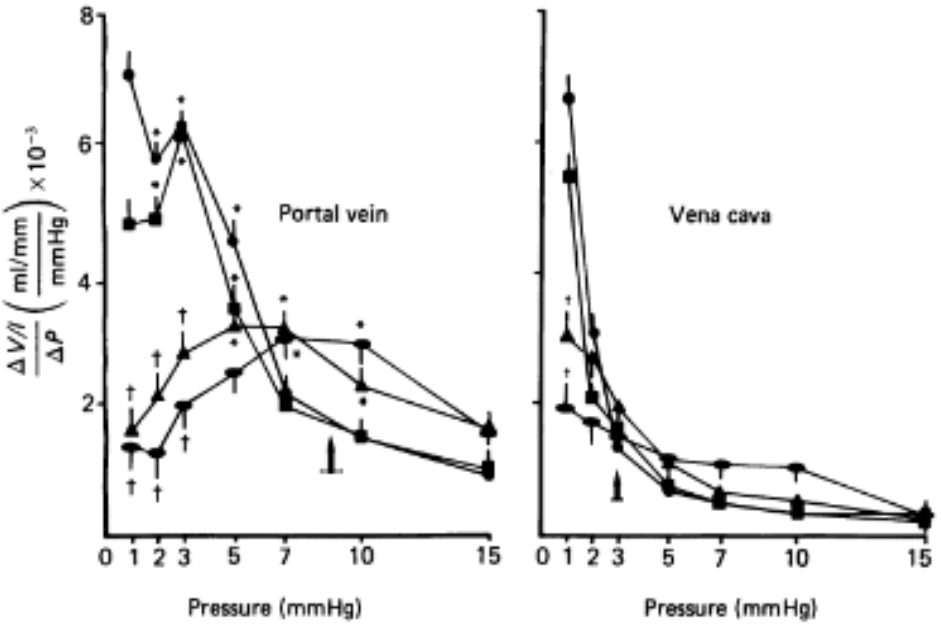

Figure 6: Compliance versus distending pressure in portal vein and inferior vena cava with a control, vessels activated in calcium-free media and with muscle activated by varying amounts of a noradrenaline. [18]

Equation 2 shows the relationship between the critical buckling pressure within the vessel with Young's Modulus, inertia, and radius of the vessel.

$$(p_r - p)_{cr} = \frac{3EI}{R^3} \qquad \textit{(Equation 2)}$$

Biological tissues are known to be hyper-viscoelastic solids which tells us that they are both elastic and viscous solids, different proportions for different vessel tissues. Viscoelasticity is a property in cardiovascular tissues that shows the material has elastic and viscous regions. Elasticity, viscosity, and viscoelasticity can be measured using mechanical testing of the dynamics of tissue's deformation to an applied load. Hyper-elasticity is the rate-dependent response of materials at very low strain rates.

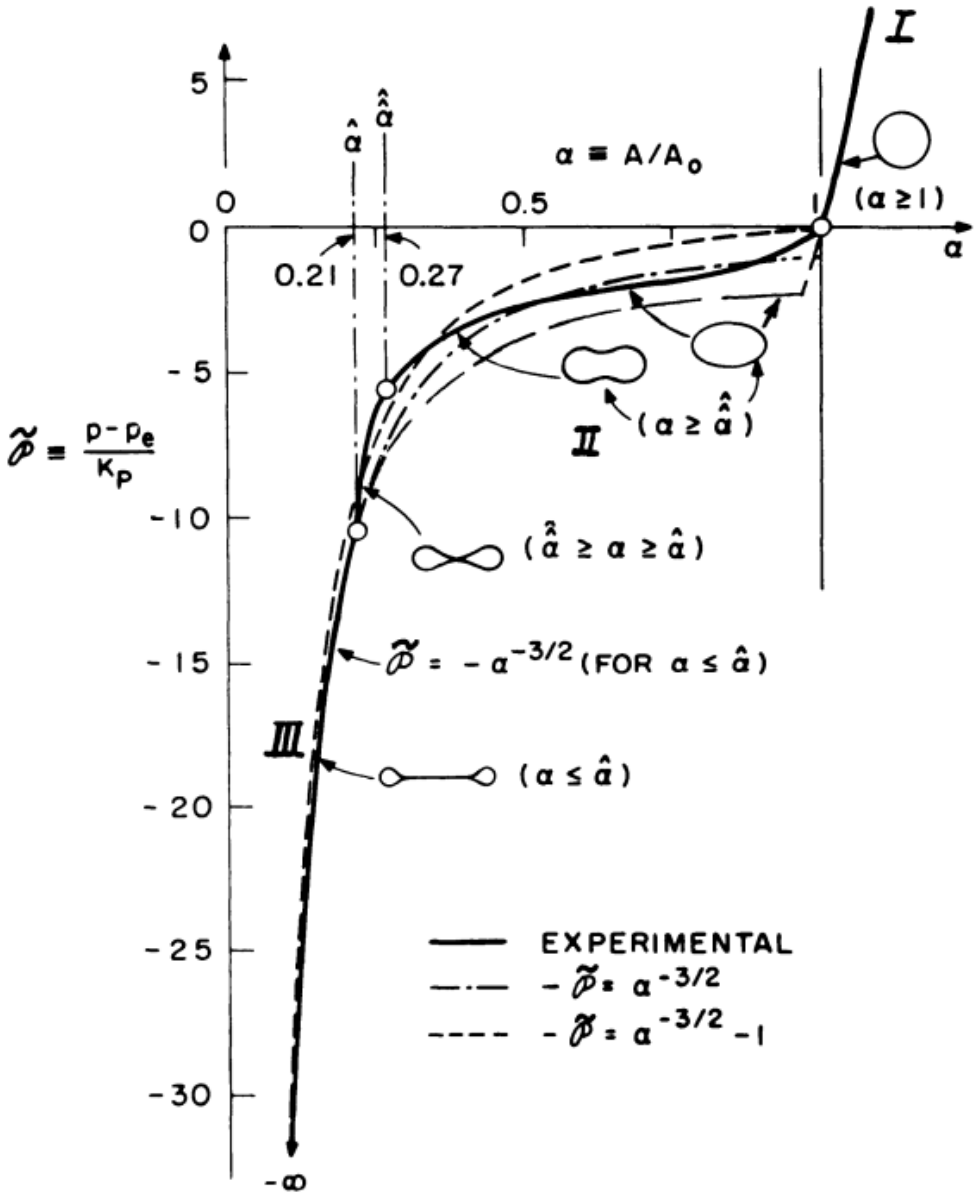

Figure 7: Behaviour of a collapsible tube. [1] Dimensionless transmural pressure difference versus reduction in diameter.

Viscoelastic materials dissipate energy upon deformation which can be seen through hysteresis in the stress-strain curve. The viscoelastic material's loading and unloading behaviors depend on the strain rate.

As shown in Figure 6, the IVC tissue undergoes a certain stiffening at a certain internal pressure within the vessel which is unique to venous tissue.

Figure 8: The Maxwell Model [7]

A Maxwell model can be used to describe the viscoelastic properties of tissue as shown in Figure 8. It includes an elastic and viscous element in series using a linear spring and dashpot. It cannot reflect the total recovery of viscoelastic materials but the elastic recovery [7].

Creep and stress relaxation experiments are used to test viscoelastic behaviors. Stress relaxation experiments require preconditioning of the sample, and a constant strain is applied while measuring the time-dependent stress reduction [19]. With each subsequent cyclic load, the internal structure aligns with the direction of the loading and the tissue dissipates less energy.

2.4 Hemodynamics

Hemodynamics is the study of the relationship between pressure, resistance, and the flow of blood through the cardiovascular system. The resistance of the flow depends on the viscosity of the fluid flowing, and the dimensions of the vessel it is flowing within [4].

2.4.1 Blood flow relationships: velocity, pressure, and compliance

Using Poiseuille's Law and Darcy's Law for relationship between pressure head, resistance, and flow rate: the flow can be determined using Equation 3.

$$Q = \Delta P \left(\frac{\pi r^4}{8VL} \right) \qquad \textit{(Equation 3)}$$

Equation 3 demonstrates the effect of the changes in radius on the flowrate in the vessel. Small changes in radius result in large changes in blood flow through the vein.

2.4.2 Biphasic Flow

Wexler in 1968 conducted a study on health un-sedated human volunteers to investigate the blood flow patterns within the vena cava. Before this study was conducted, only studies had been done on animals such as dogs. The instrument used in this study was a catheter-tip electromagnetic transducer which is passed through the right atrium to the hepatic portion of the inferior vena cava. [14]

From this study it was found that the venous velocity was extremely pulsatile within the inferior vena cava. Certain respiratory maneuvers such as the Valsalva and Muller were assessed with regards to velocity and pressures within the vena cava which is not possible in animals.

Smith in 1985 investigated the velocity patterns within the inferior vena cava using duplex scanning (real time ultrasonography and pulsed Doppler velocity measurement). The investigation found that at atrial diastole two forward facing peaks had jone due to ventricular systole (S) and the other due to ventricular diastole (D) with a negative peak at atrial systole (A) as shown in Figure 9. It was also found that respiration would influence the height of the D wave, with the start of inspiration leading to an increase in the size of the D wave.

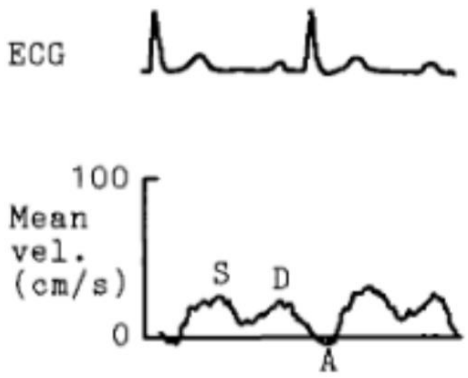

Figure 9: Inferior vena caval mean velocity pattern in a patient with normal right heart. Forward velocity waves during ventricular systole (S) and ventricular diastole (D). Negative velocity wave during atrial systole (A). [9]

2.5 Anatomy Modeling: Phantoms for PIV analysis

Phantoms are artificial mimicking structures of human anatomy for analysis of certain anatomies when in vivo measuring is too difficult or impossible. The medical device industry requires phantoms for stages of device development and proof-of-concept that the device functions correctly.

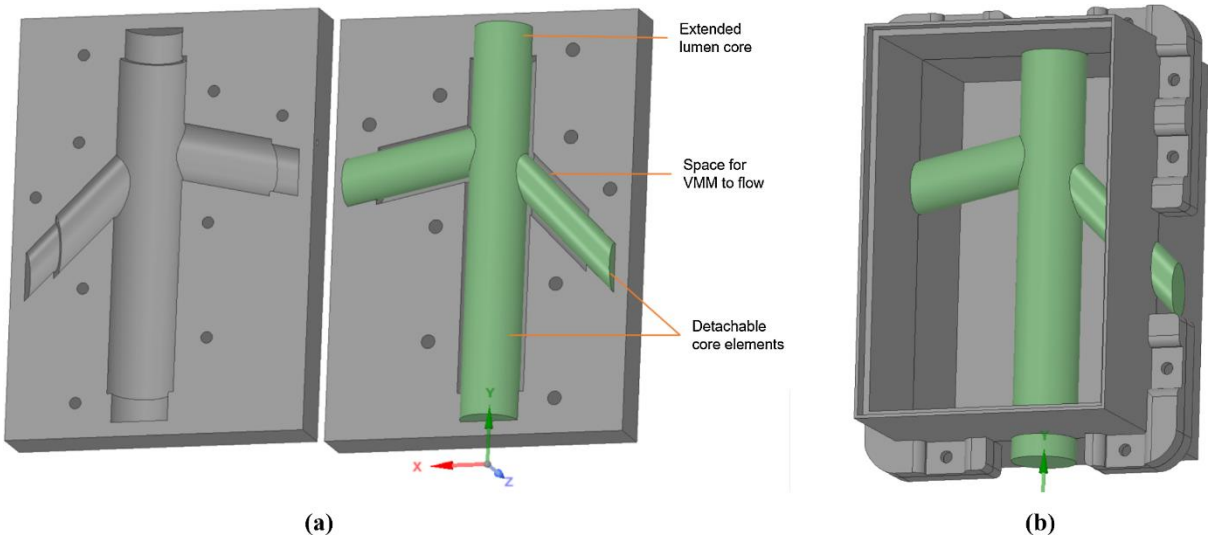

Figure 10: Lost-core casting method to create walled phantom using vessel-mimicking material in a) and tissue mimicking material to be used in b)[6]

2.5.1 Methods of Fabrication

With such advances in 3D printing and polymer materials, there are numerous ways to model anatomies as shown in the literature. PolyJet printing using TangoPlus FullCure, a rubber photopolymer for cardiovascular modelling has been shown in a study by Biglino (2013) [21].

An interesting study done using PVA-c cryogel to obtain a vessel and tissue-mimicking phantom by Nisar et al (2020) [6] for intracardiac and intravascular studies. This phantom was used to measure blood flows using ultrasound imaging which does not require the higher optical clarity that PIV requires. The anatomy and function of the IVC is produced using two alternative materials to mimic the vessel-like properties and surrounding tissue as shown in Figure 10. Figure 10 a) is a common method to produce “wall – only phantoms”.

2.5.2 PIV Analysis

Due to the location of the inferior vena cava, direct flow measurement is too difficult to obtain fluid velocity measurements. Therefore, indirect in vitro methods will be used.

To understand the hemodynamics within the Inferior Vena Cava, due to the complexity and near impossible in vivo methods, in vitro methods are used. Methods such as Doppler Ultrasound (DUS) and Magnetic Resonance Imaging (MRI) are the most common techniques. Problems arise with MRI and DUS such as angle dependence and poor resolution [22]. A more reliable in vitro experimental technique is optical PIV analysis.

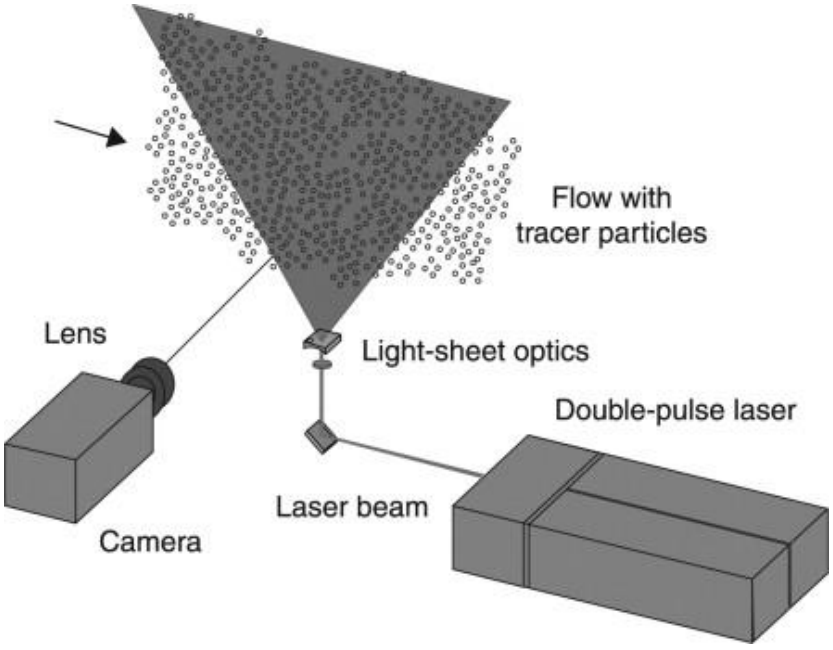

Figure 11: Diagram of PIV analysis function using double-pulse laser and high speed camera to capture planar velocity field [23]

PIV Analysis is an optical measurement technique that uses a laser image to obtain a velocity field of an entire region. Subsystems for PIV analysis include the flow test rig, seeding generator, pulsed laser system with light sheet optics, CCD digital camera system, and data acquisition/processing software. This project will deal with the flow test rig parameter, to ensure optical access to the fluid flow.

2.6 Elastomers: Polydimethylsiloxanes (PDMS)

Polydimethylsiloxane is a silicone elastomer which is very often used for microfluidics and micro-engineering devices due to its high chemical inertness, high optical clarity and mechanical properties [24]. For PIV Analysis, high transparency is required and PDMS materials are often used.[24] The tuneable mechanical properties of PDMS's hold very useful to biomedical applications and mechanobiology to mimic muscle and human tissue. The hyper elastic property of elastomers is one reason for their popularity due to their recovery when force is applied to them.

2.6.1 Sylgard-184

Sylgard-184 (Dow Corning) is a PDMS silicone that is one of the most used materials for PIV analysis due to its low refractive index water mixed with glycerol to mimic blood. Sylgard-184 has been used in flow phantoms as shown by Geoghegan (2012), Hopkins et al (2000) and Spence et al. (2011) [25] [26, 27]. Sylgard-184 consists of a pre-polymer (base) and cross-linker (curing agent) that are recommended to mix 10:1 by Dow Corning. Khanafer and Johnston show that the mechanical properties differ with different mixing ratios and the curing temperature of the elastomer [28, 29]. Sylgard-184 will be tested to improve the tear strength, optical clarity, and compliance from previous Dragon Skin™ phantom models and allow for PIV hemodynamic analysis.

2.6.2 Tear Resistance and Elongation at Break

From previous work done by UCD students, Dragon Skin™ FX PRO material was used for the IVC phantom. This material did not offer suitable compliance and optical clarity for PIV analysis. Table 1 provides an overall comparison of mechanical properties of different elastomers. For higher optical clarity one may be sacrificing a higher tear strength as Sylgard-

184 shows to have the lowest tear strength. Design considerations must be implemented to prevent fracture/tearing.

Table 1: Mechanical Properties of Select Silicone Elastomers Recommended for Fabricating Stretchable Devices [5]

elastomers	elongation at break (%)	tear strength (N/mm)
Sylgard-184	100	3.4
Ecoflex$^{00\text{-}10}$	697	3.9
Sylgard-186	195	12.2
Dragon Skin$^{10\ slow}$	507	22.0
MED 10-6400	484	28.2
Elastosil-M4130	449	29.2
Elastosil-M4630	787	33.8
ExSil 100	1864	42.0

2.6.2 Curing Time of Sylgard-184

Johnston (2014) investigated the variation in the mechanical properties of Sylgard-184 with curing temperatures from 25 ˚C to 200 ˚C using Type C dumbbell shaped test samples from ASTM D412 [29]. Results included that the Young's Modulus, Ultimate Tensile Strength, and Compressive Modulus increased with increased curing temperatures indicating higher cross linking within the elastomer material. The heat propagation through the samples was accounted for and an additional 13 minutes was added to the curing temperature provided by the manufacturer for the temperatures investigated.

2.6.3 Refractive Index

Index matching is required for successful hemodynamic analysis using PIV systems with water initially as a blood-mimicking fluid. Geoghegan (2012) uses a mixture of water and glycerol based off calculating the Womersley number to solve for fluid structure interactions [25].

Yousif (2009) undertook a challenge of refractive index matching a fluid with similar dynamic viscosity to water while matching the refractive index of Sylgard-184. A refractometer is incorporated into the flow loop to adjust the proportions of glycerol, water, and sodium iodide salt. The Sylgard-184 phantom showed to have an index of 1.4132 and the fluid within was adjusted to this value [10].

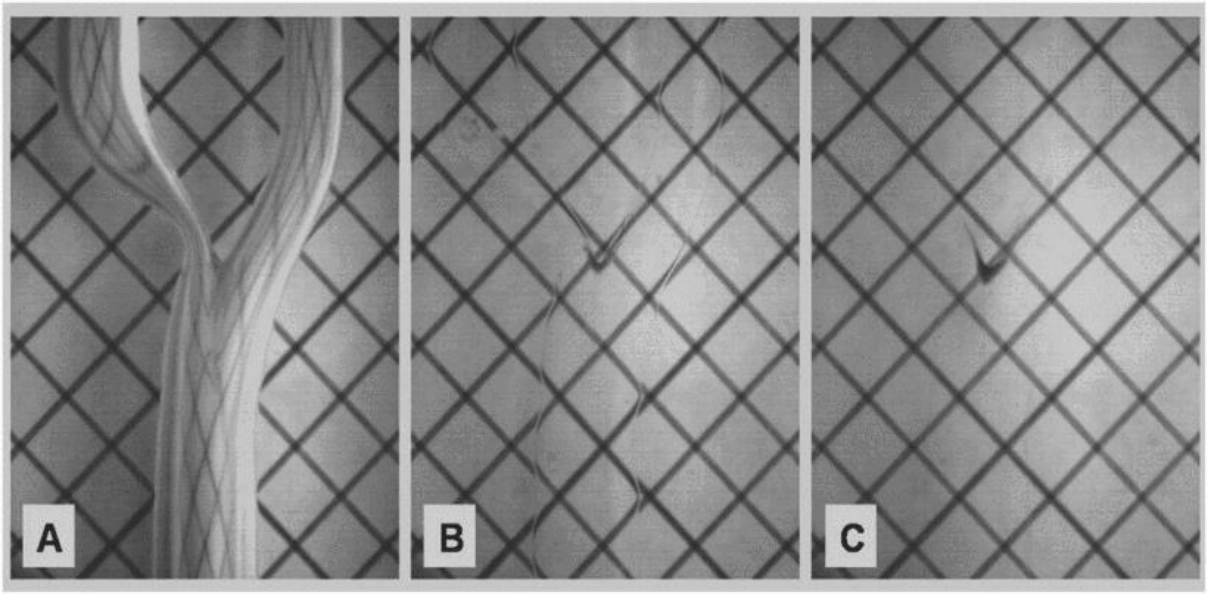

Figure 12: Grid lines below phantom to index match the phantom and fluid within phantom for successful PIV analysis. Distortion between grid lines indicates poor index-matching. A) air within model, high distortion, B) nearly matched fluid within model, C) optimally matched fluid – no distortion (n = 1.4140)[10]

Perspex container is used to contain the phantom model and therefore the fluid within the solid phantom and the phantom itself should be as close to the refractive index of the Perspex container as possible to ensure little light refraction. A refractometer can be used to determine the refractive index of the Sylgard-184.

2.7 Testing

To understand the mechanical properties of materials used to simulate human tissue, it is useful to put silicone alternatives under cyclical loading using uniaxial testing to understand its stress-strain relationships.

Silicone elastomers show properties that are looked for physically and mechanically in many applications. For a model of high bio-fidelity, the mechanical properties of the phantom must be as close to the properties of venous tissue. Cyclical tensile testing and tear strength testing are two testing methods to be assessed and implemented to appropriately prepare the phantom material.

Various variables will be monitored in the testing such as strain rate, number of cycles, temperature, strain amplitude.

2.7.1 Cyclical Uniaxial Loading

Dynamic mechanical loading is used in tissue engineering when testing tissue-engineered blood vessels composed of living vessels. This report uses the tensile test rings that are used in these dynamic mechanical tests.[3]

Due to the viscoelastic properties of cardiovascular tissue, the simple uniaxial pull to failure testing is insufficient due to the strain-rate dependent property of the material. Stress relaxation testing is used to account for this as shown in Fung and Wang [19, 30]. Stress relaxation is when a sudden strain is put on a body and maintained, and loading is applied after a certain amount of time. This is called cyclical loading and a hysteresis loop is seen in the stress-strain curves of viscoelastic solids when stress relaxation experiments are done. Preconditioning is very important for repeatability of tensile testing as it ensures the material has been under equal stress before starting the tests [31]. A preconditioning of 5% strain was used in studies done on collagen gels used for tissue engineered blood-vessels (TEBV)

5 mm wide rings of tissue-engineered tubular constructs were dynamically tested using the apparatus shown in Figure 13. A fixed strain rate of 0.2 mm/s was chosen, and the gage length was the hook-hook distance. The tissue rings were preconditioned with three cyclical loading cycles reaching 10% failure strain before testing.

Stress relaxation tests help to understand the viscoelastic properties of the tissue/material being used for the phantom.

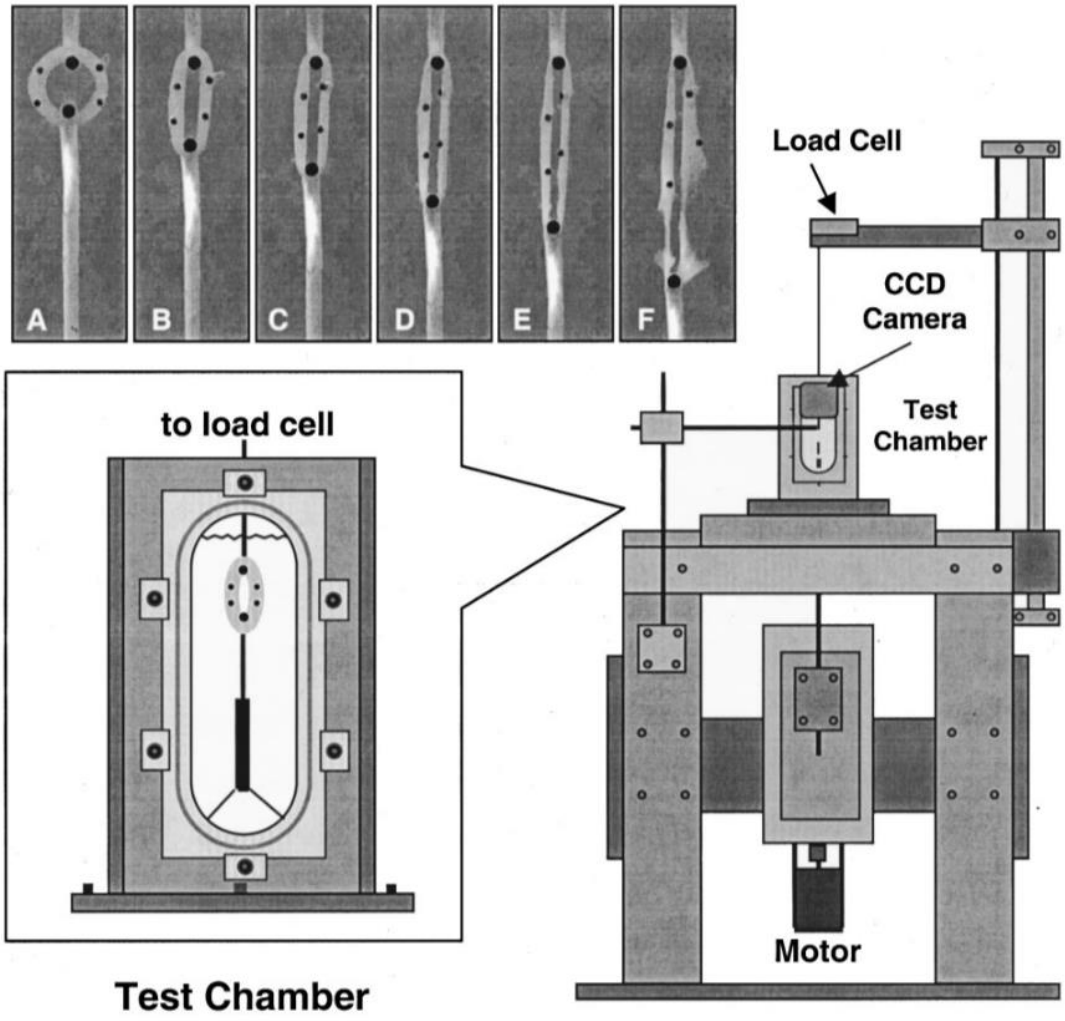

Figure 13: Dynamic Mechanical Testing apparatus to load ring samples of tissue-engineered constructs.[3]

2.7.2 Tear Resistance

From previous work done by UCD students on phantoms of the IVC, a significant problem with the use of the elastomer – Sylgard-184 is the tear strength of the material. Factors such as curing temperature and curing agent ratios affect the mechanical properties of the material.

Physiological forces of blood flow through the vessel and from tissue external of the vessel results in stresses on vessel walls such as circumferential stress, wall shear stress, longitudinal

stress due to tethering and internal longitudinal stress [11]. The material must withstand these stresses, cyclically to not fracture.

2.7.3 Compliance Testing

Gasser describes compliance as a capacity (m^3 Pa^{-1}), the ability to hold a volume of blood, a reservoir function. Equation 4 shows volumetric compliance described by Gasser, [17].

$$C = \frac{\Delta V}{\Delta p} \qquad \textit{(Equation 4)}$$

A study done by Colombo et al. (2010) investigated the effects of curing agent ratios and temperatures on the compliance and mechanical viscoelastic strength of Sylgard-184. Using hydrostatic luminal pressure, the vessels were inflated at certain pressures (0-200 mmHg), using a video extensometer, cyclical strain and external diameter at each pressure stage was measured [32]. It was found that the compliance of the vessels increased with higher ratios of polymer base to curing agent from 10:1 to 16:1.

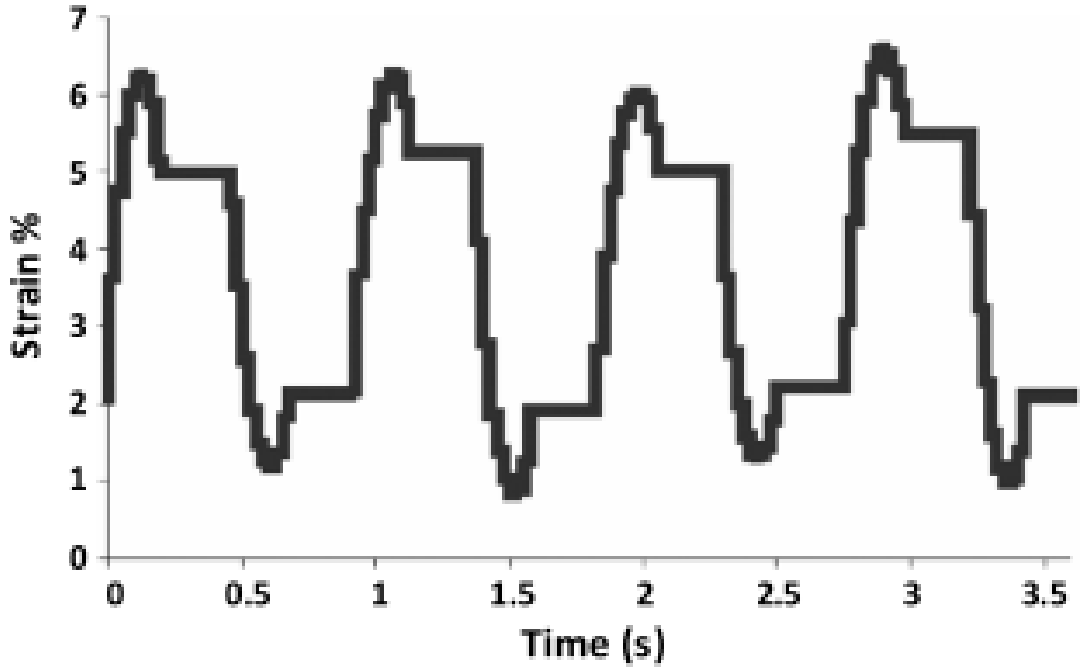

Figure 14:Strain % cycles of Sylgard-184 artery phantom under heartbeat pressure cycle recorded with video extensometer.

3. Methodology

3.1 Chapter Layout

This chapter will discuss the methodology behind the project's objectives. This will include the methods behind designing the samples for testing, model prototypes and development of the designs throughout this project.

Section 3.2 will go through the design process of developing sample rings for Sylgard-184 tensile testing. Section 3.3 will discuss the development of the design of the mold for the right heart simulator model of the IVC. Section 3.4 will discuss the method of molding Sylgard-184 along with specific methods for the final mold produced. Section 3.5 will discuss the methods used for tensile testing of Sylgard-184 rings and methods used for nonstandard investigatory testing of defective models.

3.2 Sylgard-184 Ring Mold Design

3.2.1 Problem Statement

Creating samples of Sylgard-184 that are accurate and repeatable, an injection mold must be designed that can accommodate for shrinkage when curing the material at different temperatures, the surface finish must be appropriate, and the mold is to be reused for additional samples.

3.2.2 Design Process

A ring design is used to minimize the slipping of the sample when testing cyclically. Pin mounts are used to hold the ring and stretch it outwards. Additionally, the function of the testing is to understand the viscoelastic properties of the vessel transversely. Studies carried out on tissue engineered vessels utilize this method of sample design.

After assessing the surface finish of 3D printing methods available to use in UCD, it was concluded that SLA printed molds would provide the accuracy and surface finish needed for the samples for cyclical testing. FDM printed PLA was tested and compared. The mold release agent requires a smooth surface and by using SLA printed molds with high resolution and layer height, this improves the surface finish. The FormLabs 2 printer has an accuracy up to 0.025 mm which is higher than the average tolerance of 0.1 mm for a standard Prusa FDM Printer.

The dimensions of the rings of Sylgard-184 are based on the original purpose of the model for the right heart simulator, mimicking the anatomy of an animal-sized IVC. The internal diameter of the mold design is 12.7 mm with wall thicknesses of 1.5 mm, and a length of 20 mm.

To adapt and compare the results from the cyclical testing done using the smaller diameter vessel, the data will be normalized by the diameter of the rings. It was decided to use an aluminum mandrel eventually to be used in the mold since it would improve the surface finish, reduce the stress applied for ring removal.

3.2.3 Ring Mold Iterations

Iteration 1:

A resin printed mandrel and two external shell molds were printed. The location of risers and runners were not appropriately placed, and alignment integrated into the design was absent. Clamps were applied externally to reduce leakage.

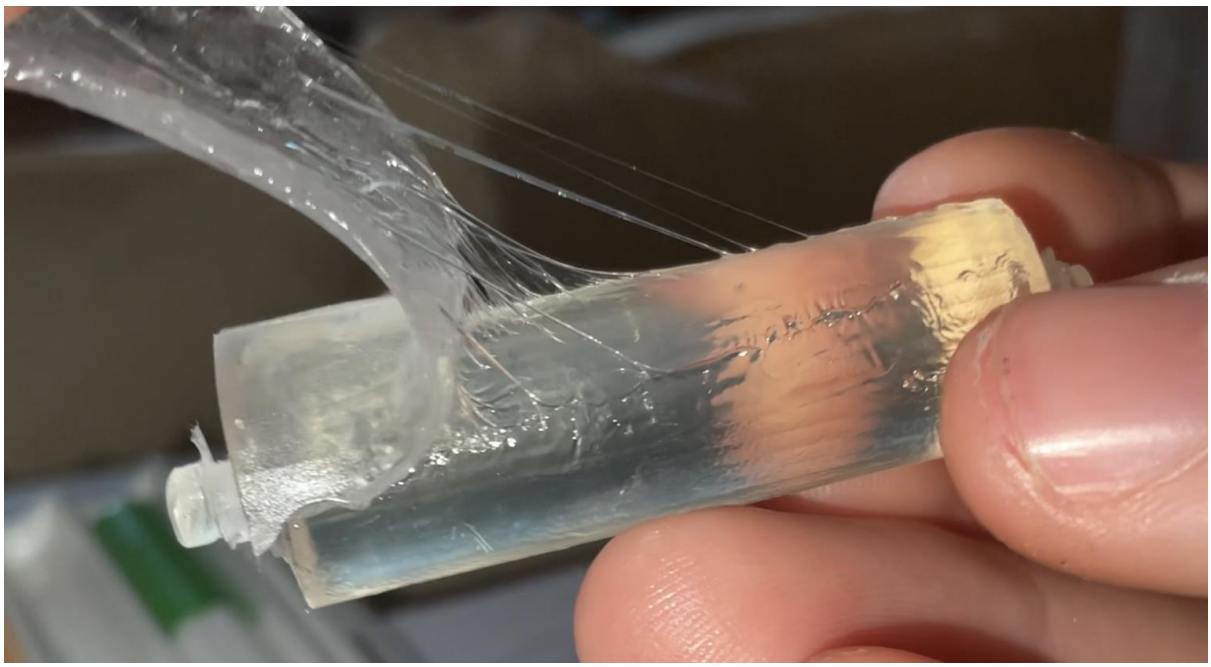

Figure 15: Iteration 1, uncured Sylgard-184 from excess release/inhibition agents

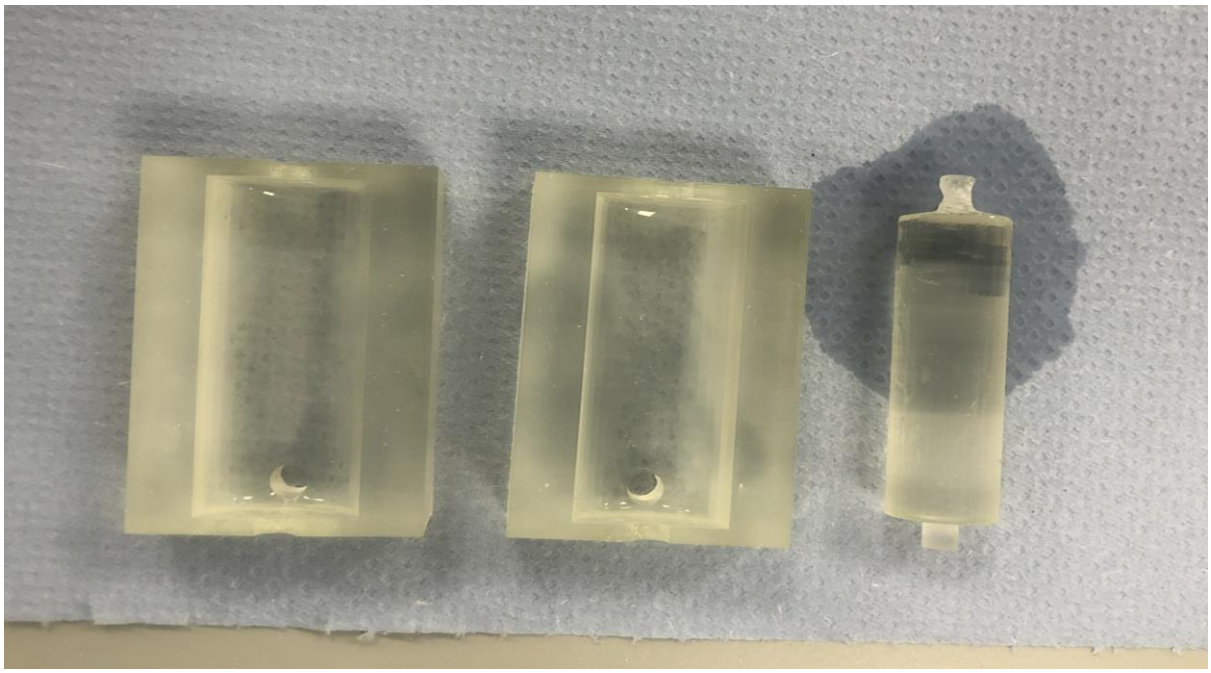

Figure 16: Iteration 1, silicone ring mould design. Resin printed (Formlabs, V4) mandrel and two external molds.

Iteration 2:

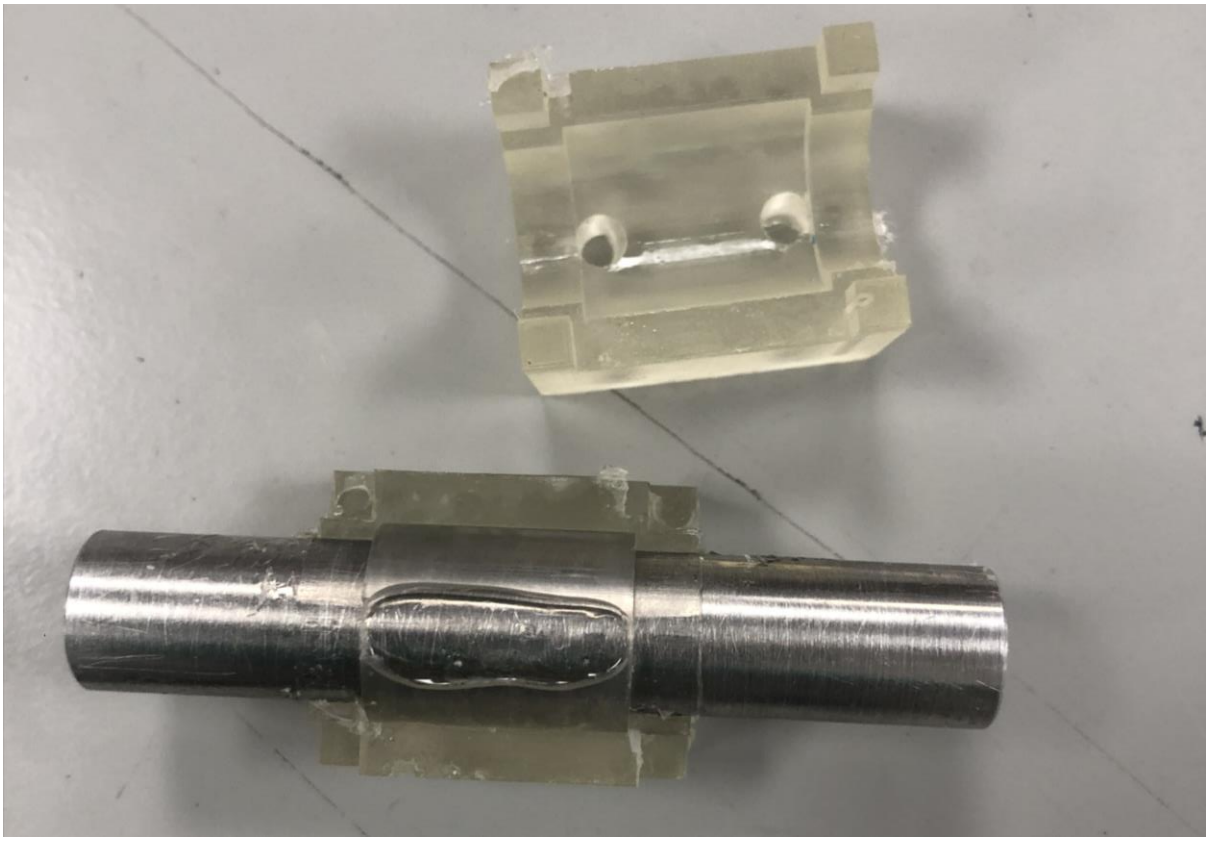

Figure 17: Iteration 2 design, incomplete ring formed due to shrinkage.

Utilizing features from previous master's students [33]who had done similar work with an alternative material, the mold was redesigned. Features such as the interlocking female/male mold design for alignment and stability/repeatability were used. The riser and runner of the mold on the same half to ensure the mold can be cured horizontally.

An aluminum mandrel was used as seen in Figure 17. As shown in this image, the silicone shrank while curing and resulted in an incomplete ring of Sylgard-184. To account for this a reservoir/ larger riser was used to feed silicone into the mold cavity to prevent these results from occurring. The interlocking mechanism was an improvement although the two surfaces were not 100% mating due to the surface finish and tolerancing of locking mechanisms.

Iteration 3:

To allow for the polishing of the SLA surface to allow for better mating between the two molds, the design was changed to allow for alignment using dowel pins. A further addition was the increased number of rings produced per mold to increase the number of samples produced for each molding. Figure 19 shows the changed design to improve the mating between the molds and reduce the seamline of the resulting ring. Figure 18 shows the additional ring produced by the mold.

Figure 19: Iteration 3, utilizing dowl pins to align the moulds.

Figure 18: Further developed ring mould to produce 2 rings in one mould.

3.3 Right Heart Simulator Model Mold Design

This section will go through the development of the external molds and mandrel for designing the IVC model. It also includes techniques used to improve certain materials' surface finish and methodologies that have changed due to undesirable results mentioned in Section 4.2.2.

Section 3.3.2 will discuss the dimensions used for the final mold design and reasoning for this. Section 3.3.3 will discuss the mold design, methods of improving the PLA previous molds, discussing features of previous molds and improvements made.

3.3.1 Problem Statement

For repeatability and accuracy, a mold for injecting the elastomer is designed to allow for high accuracy, surface finish and for easy attachment and detachment to the right heart simulator. A mold design should allow for the testing of alternative silicones without variation. The model must be altered to be attached and detached from the right heart simulator.

3.3.2 Tube Design

The previous tube model used was a tube with an inner diameter of 14 mm with ranging thicknesses. This diameter is related to the inner diameter of animal anatomy.

The final model has a 20 mm diameter to test the model at human anatomy pressures and cycles, therefore using human dimensions for the IVC. A thickness of 2 mm was chosen to produce the model as it was learnt that it would be less likely to tear and to ensure the success of producing a standard model to begin testing with. Slight under sizing of the end connectors was decided to prevent the tube from slipping.

3.3.3 Mould Design

Utilizing the printed mold and mandrel designed by Oisin Byrne in a previous thesis project to mimic the compliance of the Inferior Vena Cava using DragonSkin Silicone, as a primary design to understand the requirements for the design of the mold for Sylgard-184 [33]. These mold/mandrels were used to quickly problem solve regarding the requirements and issues with molding Sylard-184.

The previous mandrel had a 14 mm internal diameter with outer molds resulting in a 1.5 mm thick model of the IVC.

Model Mold Iterations: Prototype 1

Problem Statement:

To way to mold Sylgard-184 with previously designed molds used for DragonSkin Silicone alternatives. A way to improve the surface finish of PLA molds for silicone release.

Solution: Preparation of Molds (PLA, FDM printed)

The PLA molds were shown to have a rough finish that would not provide a smooth surface for the Silicone Release Agent. Ways of improving the surface finish of these molds were investigated.

Methods Used:

- Sanding

Sanding the molds inner surfaces using SiC sheets, beginning with low grit numbers of 340 to higher grit numbers of 2600 to reduce the scratch marks from the sanding paper. Water was used as a lubricant to reduce the aerosol particles produced and improve the sanding process.

- Resin Coating

Figure 20: RS EL2 Laminating Epoxy Resin used for improving surface finish of mould surface.

Attempt to improve the surface finish using EL2 Epoxy Resin, a resin with highest viscosity available in the mechanical laboratory in UCD. This was used to coat the inside of two mold's surfaces. Using a fine brush and heating the resin at 30 C for 40 minutes, for each layer of epoxy added to the surfaces.

- Mold Release Wax

Mold Release Wax (Miracle Gloss Mould Release Wax 8) was used to fill in the gaps of the PLA mold and provide an additional method of releasing the silicone from the mold post-curing. Gloves were used in a fume cupboard when applying the wax to the mold.

- Epoxy Resin and Filler

Finally, boat filler and epoxy were used to increase the viscosity of the epoxy coating and prevent accumulation at the base and corners of the mold. It was painted onto the mold lightly and pressed using plastic sheet over the mandrel to improve the uniformity of the coating on the mold's surface. It was left to dry overnight.

Figure 21: Plastic sheet around mandrel used to press epoxy-filler onto surface for smoother finish.

Molding of Sylgard-184: Prototype 1

The two molds were filled with mixed and degassed Sylgard-184 and placed back into the vacuum chamber to ensure no air bubbles remained. The mandrel was inserted into one mold and the other mold was quickly clicked into place on top.

Clingfilm was used to wrap/seal the mold before putting it into the vice for curing. After the curing time was reached (48+ hours), the clingfilm was removed, one external mold is taken off the mandrel slowly and carefully to ensure the silicone does not stick and tear, followed by the second external mold. The mandrel splits directly in the center. Using Isopropanol, between the mandrel and the silicone, the mandrel is twisted with small movements to ensure large shear stress is not applied to the silicone model.

Figure 22: PLA moulds filled with Sylgard-184 in vacuum chamber for second round of degassing stage.

Prototype 2:

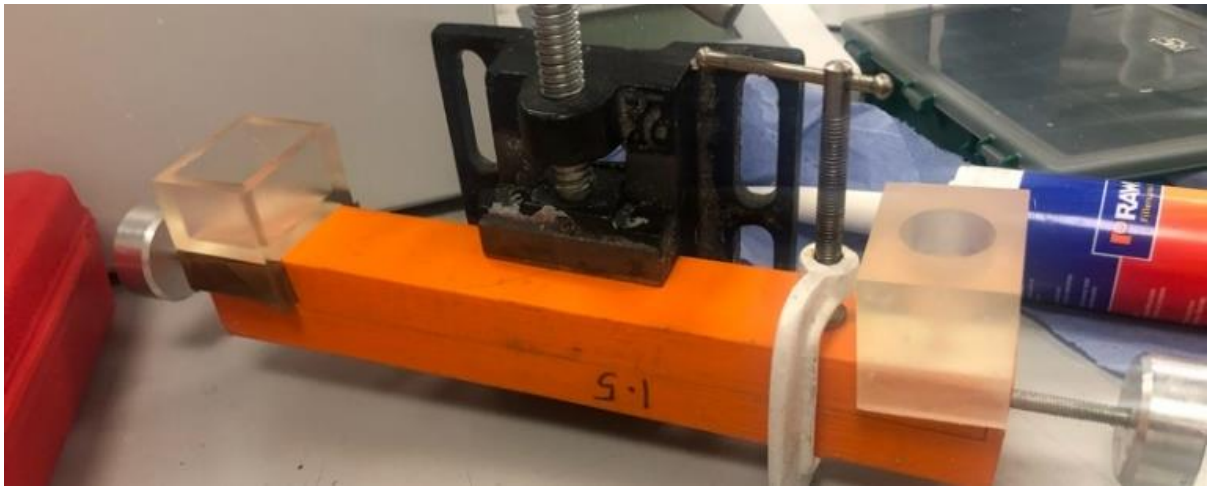

Figure 23: Added reservoirs to mould to introduce material while curing to compensate shrinkage.

Problem Statement:

A way to seal the two molds containing the aluminum mandrel, to minimize silicone waste and reduce the air introduced into the mold through shrinkage. A way to inject Sylgard-184 into the mold, reusing the molds from previous prototype 1.

Solution:

As shown in Figure 24. reservoirs of silicone were 3D printed using the FormLabs 2 printer using clear V4 resin. Two clamps were required due to the flexibility of the PLA molds and to minimize gaps between the male and female molds. Caulk sealant was used to replace the cling film as an alternative method of reducing the wasted Sylgard-184 and ensure no leakages. Two 5 mm holes were drilled into the top mold at either end as a riser and a runner for the injection process.

The runner is located on the right in Figure 24, where the elastomer is injected using a 60 ml BD syringe, slowly. The molds are kept horizontal for the injection process and the air is pushed through the mold until Sylgard-184 is seen rising through the hole on the LHS shown in Figure 24. The two reservoirs are filled with Sylgard-184 to ensure the mold is kept full and prevent the intake of air if there is leakage or shrinkage.

After the curing time is over, using a blade, the excess silicone in the reservoirs is removed to free the model from the top external mold. Next, the top mold is removed, using the vice to

stabilize the base mold. Following the same steps mentioned in the methodology for Prototype 2, the mandrel is removed from the base external mold.

3.4 Sylgard-184 Molding and Preparation

3.4.1 Problem Statement

To guarantee the removal of potential variability in mechanical and material properties in the right heart simulator and the compliance/cyclical testing, Sylgard-184 samples and models must be produced using a constant, repeatable process.

3.4.2 Method: Ring Molds

1. Predetermine the volume required by using CAD or other software to determine the volumes required of Part B and Part A of Sylgard-184.

2. Set weighing scales to zero.

3. Using pipette measure out specific quantity of Part B

4. Using scale of 10:1 for Part A: Part B – weigh out Part A into container with Part B using a wooden stick to control the viscous substance into the container.

5. In a fume cupboard, mix Inhibition reagent (Inhibit X) into a container containing the external molds and mandrel. This will prevent the attachment of the mold to silicone. Allow the reagent to dry for 10 minutes.

6. Spray mold release onto external molds and let dry for 5 minutes, in the fume cupboard. This is to allow for easier release of samples from the mandrel and external molds. Apply a second coating and lightly brush with a fine paint brush to remove excess mold release.

7. Taking container with Sylgard-184 – place into the ThinkyTM ARE 250 mixer for 90 seconds for complete mixing of Part A and Part B.

8. Place container into degassing chamber as shown in Figure 23 for 45 minutes. Air bubbles should be seen leaving the silicone throughout this process.

9. After degassing – using a syringe and ensuring no air in the syringe prior – fill the syringe with the Sylgard-184.

10. Using clamps and horizontal surfaces, place the external molds and the mandrel together and ensure they are aligned with no gaps.

11. Inject the Sylgard-184 into an injection hole in the external mold until the Sylgard-184 exits the internal cavity through the alternative hold on the mold. Inject slowly into the cavity.

12. Pre-heat vacuum oven to the desired curing temperature.

13. Place clamped molds with Sylgard-184 into oven and leave for the calculated curing time (considering heat propagation)

14. Remove sample from oven and leave to cool at room temperature.

15. After 24 hours remove external molds followed by unscrewing the mandrel and carefully removing silicone tube/sample.

3.4.3 Method Model Molds – Aluminum Mold

1. Skip step 5 for preparation of the aluminum for the molding process. Only mold Release is required for the molds since aluminum will not have a chemical reaction with Sylgard-184.
2. Attached the two-piece mandrel without excessive force, using a soft hammer, make sure there is no gap between the interface of the two pieces.
3. Place the mandrel inside the bottom external mold, with the cuff of the mandrel sitting on the end of the mold. Place the top mold, sitting with the “FRONT” face in-line with the mandrel’s cuff.

4. First screw the two M5 bolts into the mold to ensure they are inline and correctly positioned.

5. Insert the two dowel pins into the remaining two holes. These pins are of different size, ensure they are place in the correct hole. Due to the tight fit of the dowel pins, use a pin-pusher to ensure they are fully inserted.

6. Begin with the mold vertically, ensure it is stable for the injecting process. As shown in Figure 25.

7. Fill a 100 ml syringe to ensure there is enough material before beginning the injection process.

8. Attach the luer-locking adaptor to the Syringe that will be inserted into the mold.

9. Inject into the mold, if the force required is too much, use a caulk gun to apply a constant pressure and prevent excessive force applied.

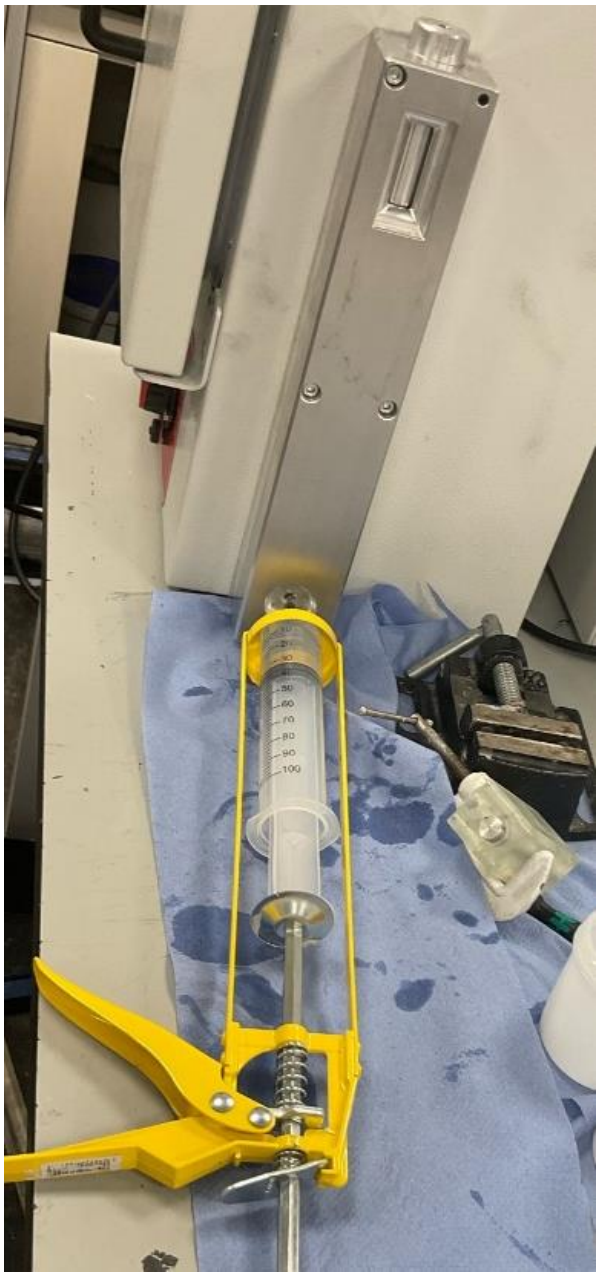

Figure 24: Injection process using 100 ml syringe into base of mould cavity while mould is placed vertically.

10. Once you begin to see material exiting the mold through the reservoir, begin to tilt the mold, to allow for the air to escape the mold through the reservoir. Until the mold is fully filled, and all the air has escaped the cavity, leave the mold fully horizontal. Leave for specified curing time at desired temperature in vacuum oven.

Figure 25: Ring and model moulds/mandrels left to dry in fume cupboard after applying Inhibition Agent (Resin prints) and Mould Release.

Removal of PDMS Model from Mandrel

1. Remove both external molds from the model/mandrel by removing the bolts and dowel pins first. This can be done using a vice holding one mold stable and levering with the mandrel.
2. Using the mandrel-splitting holder design in the UCD mechanical workshop, screw each side of the mandrel into the set-up. Turn the large bolt clockwise to release the mandrel using a suitably sized wrench, as shown in Figure 27.
3. Isopropyl Alcohol between the mandrel and model to release the model from the aluminum surface.

Figure 26: Splitting of mandrel to release model.

3.5 Uniaxial Tensile Testing

3.5.1 Problem Statement

It is desirable to design cyclical tensile tests of rings of the Sylgard-184 due to the constant pressure changes throughout the biphasic flow cycle in the Inferior Vena Cava. Understanding how the silicone response mechanically to cyclical strain will provide understanding of the controllable mechanical properties when curing the Sylgard-184 at different temperatures.

A suitable comparison of the stiffness and viscoelastic properties between DragonSkin FXPro used previously with the Sylgard-184 model would be beneficial to ensure the development of the model is in the correct direction.

The Lloyds LS1 Tensile Testing machine is used to apply cyclical loadings to the material and provide data for analysis by MATLAB after. Another aim is to investigate the strength of failed prototypes using nonstandard pull-to-failure tests of the prototypes.

3.5.2 Design of Experiments (DoE)

Hypothesis:

To investigate the effect of curing temperature on the viscoelastic mechanical properties of Sylgard-184, careful design of experiments must be done. Elastomers can lose their viscoelastic properties, resulting in a brittle and prone to cracking model.

Strain Rate and Cycle Time:

Unlike Dragon-skin which was previously used, Sylgard-184 has a relatively low elongation at break (100% strain) [5]. A strain of below 40% will be used since this will allow for the calculation of the shear and bulk modulus for Sylgard-184 using Poisson Ratios from the literature. By subjecting the samples to four cycles of below 40% strain it simulates the repeated loading and unloading that the model would experience *in vitro.* This testing will provide valuable information regarding the mechanical viscoelastic properties and durability of Sylgard-184. All conditions except curing temperature were kept constant to ensure there is no undesired variability. These factors include degassing time, mold preparation, injection process and mixing ratio of the elastomer.

To test the specimen at a certain strain we must calculate the final length to test the ring at using the engineering strain equation, Equation 5:

$$\varepsilon = \frac{(L - L_0)}{L_0} \qquad \textit{(Equation 5)}$$

3.5.3 Preparation

1. Attaching the load cell (1kN load cell used); mounting the load cell and securing using the pins attached. Hand-tighten the pins at the load cell. Switch on the machine and press the orange button.

2. Screw the top and bottom grips onto the machine and insert the pin.

3. Screw on the pin mounts.

4. Align the pin mounts to ensure uniform tension applied to the silicone rings.

5. Set the lower and top limits within the range of motion expected for the load cell for safety.

6. Move the pins manually to less than the inner diameter of the rings, using a ruler. Set to zero position when finished.

3.5.4 Method: Sylgard-184 ring samples

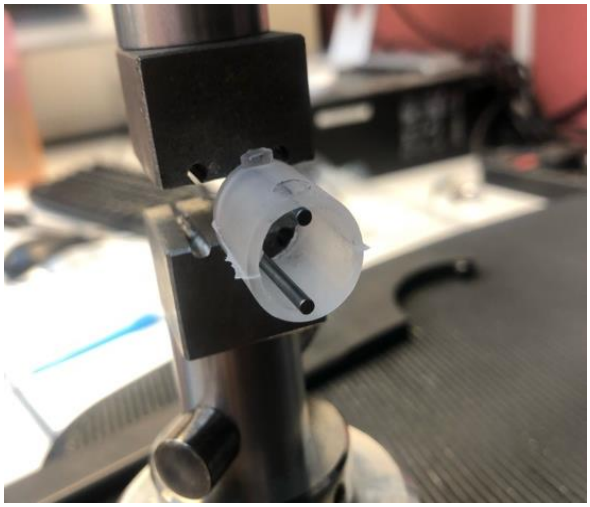

Figure 28: Slacked Sylgard-184 ring sample held by pin mounts for tensile testing.

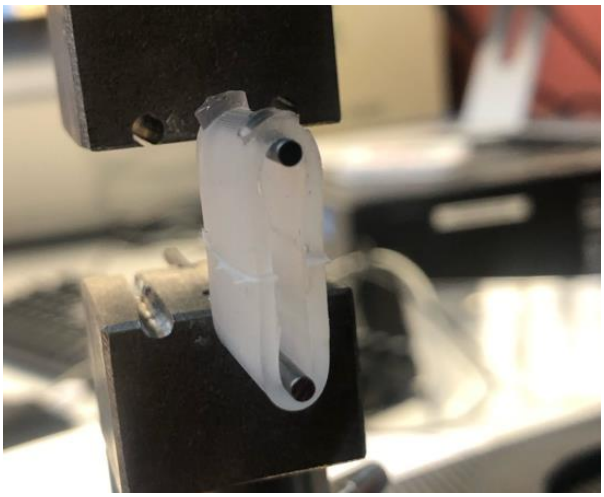

Figure 27: Taught Sylgard-184 ring sample help by pin mounts

1. Insert sample ring onto the pin mounts. Ensure the ring is slack (not under tension) and manually adjust the machine, followed by setting it to home at this position. Ensure placement of ring samples is replicated for each sample – with the seamline in the horizontal center between the pins.
2. Create a new batch of tests on NEXYGEN Software.
3. Set a preload of 0.1N to detect when the machine is beginning to put the rings in tension.
4. Gauge length was taken to be the inner diameter of the sample.

5. The cross-sectional area was taken to be the two sizes of the ring when being stretched (2 x 20 mm x 1.5 mm).
6. The strain rate magnitude was set prior to starting each test. Once 4 cycles are complete, a pull to failure test is done to understand the breakpoint / ultimate tensile strength of the material.

3.5.5 Nonstandard Tensile Tests: Pull to Failure

Nonstandard pull-to-failure tests were done on the failed prototypes, 1 and 2. This was an investigation with regards to the strength of models with defects and to see where the samples factures in relation to their defects.

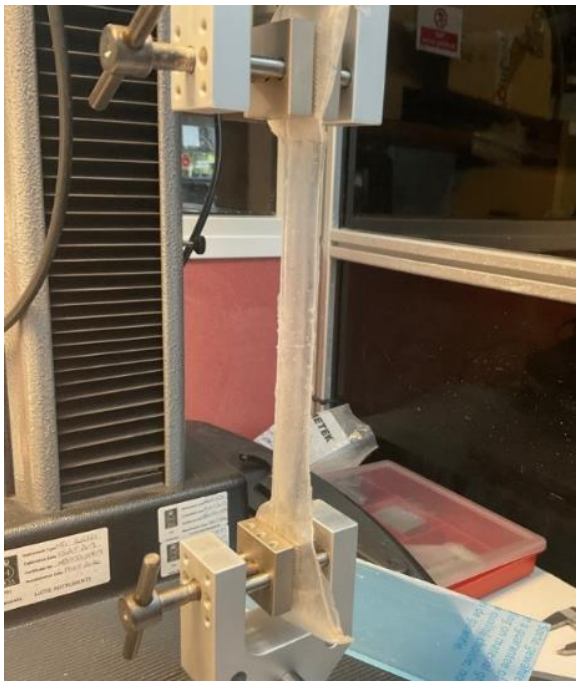

Figure 30: Prototype 1: Pull-to-failure set up for nonstandard investigatory tests of defective prototypes.

Figure 29: Prototype 2: Pull-to-failure set up for nonstandard investigatory tests of defective prototypes.

Method:

1. Follow preparation instructions, replacing the pin mounts for vice clamps to secure the models without tearing.
2. Place the clamps at the end connector sections of the model, with the gage length being the 150 mm middle-section of the model. Align the clamps with Perspex sheet, to ensure the clamps are directly below each other to prevent forces applied to the model in alternative directions (not uniaxial).

3. Ensure enough force is applied to the model to prevent slippage. Over-tightening the clamps could result in tearing the model so hand tighten until enough force is applied to hold the model securely.
4. Create a batch of tests for pull-to-failure tests at 1.5 mm/min.
5. Applying a preload of 0.2 N, begin the test and note the distance between the tops of the clamps to note the beginning gage length.
6. Analyze the force-distance data using MATLAB software for a stress-strain curve.

4. Results

4.1 Chapter Layout

Section 4.2 will discuss the results with regards to the models produced from the developing molds (PLA to Aluminum). Section 4.3 shows the set-up of the model in the right heart simulator attached to the abdominal, water-pressurized chamber. Section 4.4 shows preliminary results from inserting the model into the chamber and manually collapsing the model for investigation. Section 4.5 will show the results from the cyclical testing done on 100 C and 21 C samples. Section 4.6 shows the non-standard investigatory tensile tests of failed prototypes for additional information on the effects of defects on model strength.

Figure 31: Prototype 1, failed due to leakage and insufficient sealing of mould interfaces.

Figure 32: Prototype 1 full model - half model due to leaking between two moulds interface.

4.2 Sylgard-184 Models

4.2.1 Preliminary Models

Prototype 1:

As shown in Figures 33 and 34, the first prototype was made using previous molds [33] and aluminum mandrel with a 14 mm inner diameter. The interfaces of the molds allowed for the elastomer to escape over the curing period which the cling film couldn't contain. The alignment teeth of the molds did not fit perfectly due to tolerances of the FDM printer - resulting in small gaps between the molds interfaces.

It was observed that the elastomer shows shrinkage during the curing process resulting in a requirement for runners and risers in the design of the mold to allow for material to be drawn into the mold when shrinkage occurs. Figure 34 shows the resulting half-model due to the leakage.

Figure 33: Prototype 1 Model removed from PLA moulds.

Prototype 2:

Prototype 2 was the first fully formed tube produced. It was molded at 21 ˚C and left for 72 hours to ensure full cure before removing from the external molds. Dow Corning recommends leaving the model to cure for 24 hours at 25 ˚C but from previous mold iterations, it was safer to leave it for more than 48 hours to ensure full cure for a lower room temperature of 21 ˚C.

Observations:

- Air bubbles from insufficient degassing or else introduction of bubbles into mold through the injection process.
- Internal line at center due to the mandrel splitting at the center of the mold. Mandrel was very loose and produced visual defects that could potentially interfere with PIV analysis.

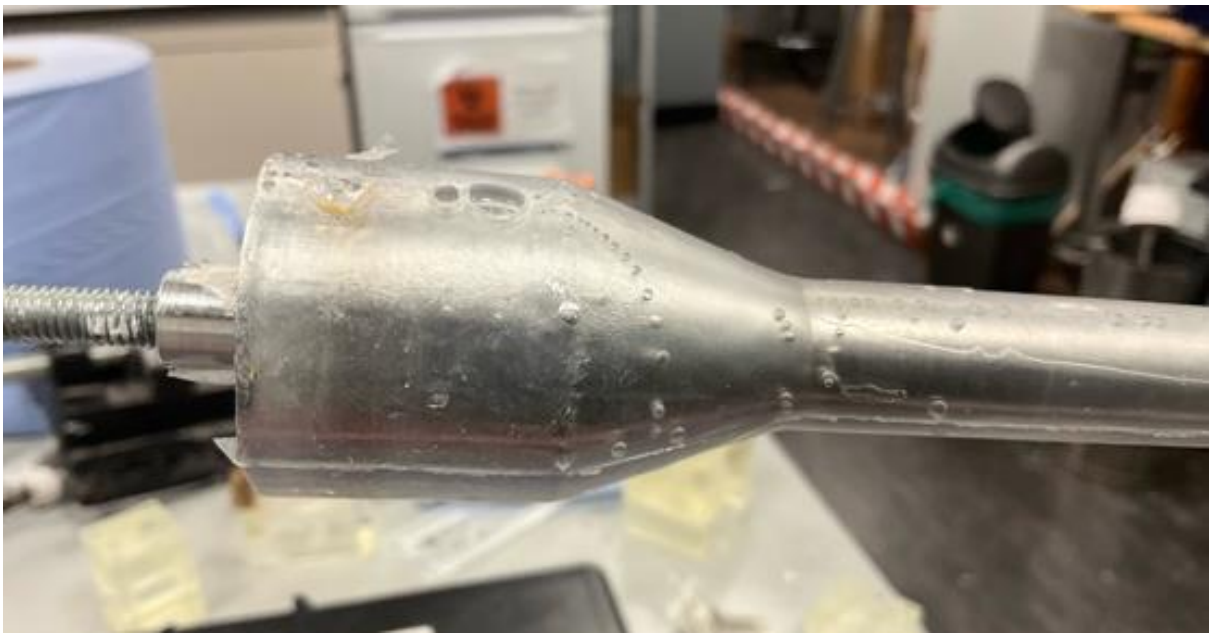

Figure 35: Defects of Prototype 2 shown: bubbles from poor Sylgard-184 degassing and introduction into mould. Trapped air bubbles, seamline, and markings from surface of PLA mould.

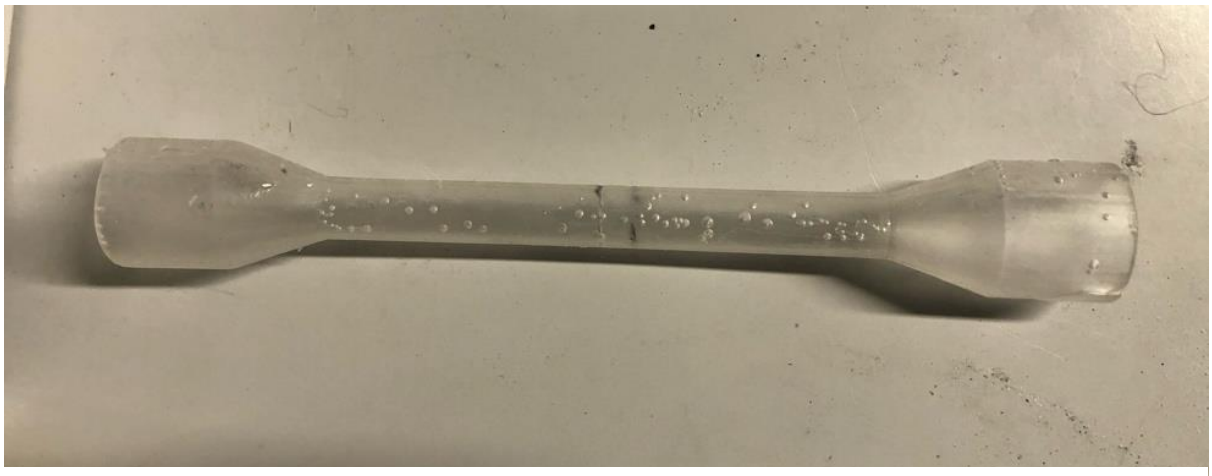

Figure 34: Defects shown in model from Prototype 2; trapped air bubbles, seamline, and slight shrinkage from injection site. Marking from split of mandrel at centre of model.

4.2 Final Models

The final models produced were cured at 100 ˚C (1 hour) and at room temperature (21 ˚C, +48 hours) to gain insight into the compliance of the two models under cardiovascular pressure cycles, Figure 37. The model ends for attaching to the rig were purposefully undersized to ensure no slipping and a secure fit. Due to the tackiness of the PDMS, it was difficult to remove and attach the model. Isopropyl alcohol between the model and the mandrel was very efficient for reducing the friction between the two surfaces and reducing strain on the models.

PLA, FDM printed connectors were produced to allow for easier removal/attachment to the chamber without wearing the delicate elastomer. An alternative method of cutting the end attachments of the model in half and using a jubilee clip was tried and worked sufficiently, using the removed Sylgard-184 as padding underneath the clip to prevent the clip from tearing the model. Two models were produced to see the difference in collapse between a stiffer (100 ˚C) model and more compliant model (21 ˚C).

Figure 36: Two final models to be placed in right heart simulator with adjusted end attachments due to fragility of Sylgard-184. Bottom was cured at 100 ˚C and top at 21 ˚C.

Due to the reduced strength of the 21 ˚C cured model, tearing occurred upon removal of the mandrel. An elastic resin printed attachment was printed (Elastic 50A, Formlabs) to recover the model for use in the right heart simulator.

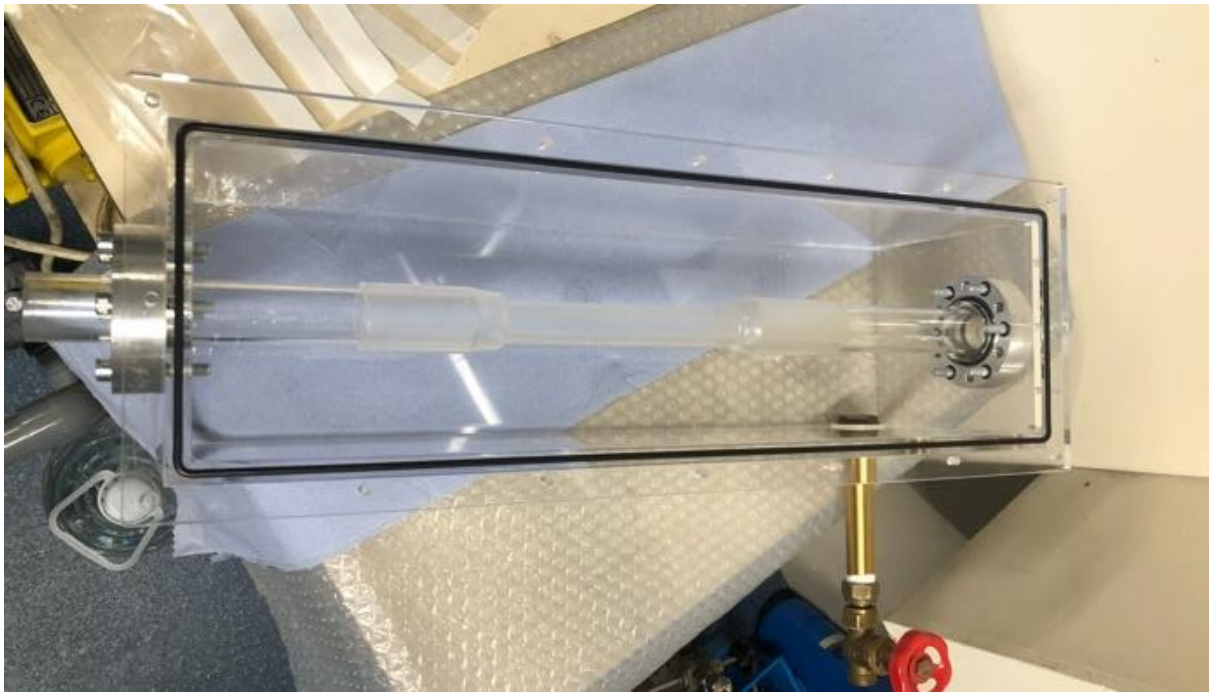

Figure 37: Attachment of model to water pressurized chamber.

4.3 Right Heart Simulator Assembly

Figures 38, 40 and 39 show the attachment of the IVC model into the water pressurized chamber for PIV Analysis. Transparency of the IVC model was tested using clean water inside the model and outside. Figure 39 shows the model in a cloudier Blood Mimicking Fluid (BMF) with higher viscosity and a better refractive index match to water.

To account for the refractive index of Sylgard-184, the fluid was matched using the literature [10, 34], glycerol was added to a ratio of 40:60 water to glycerol to refractive index the material to the fluid within and outside.

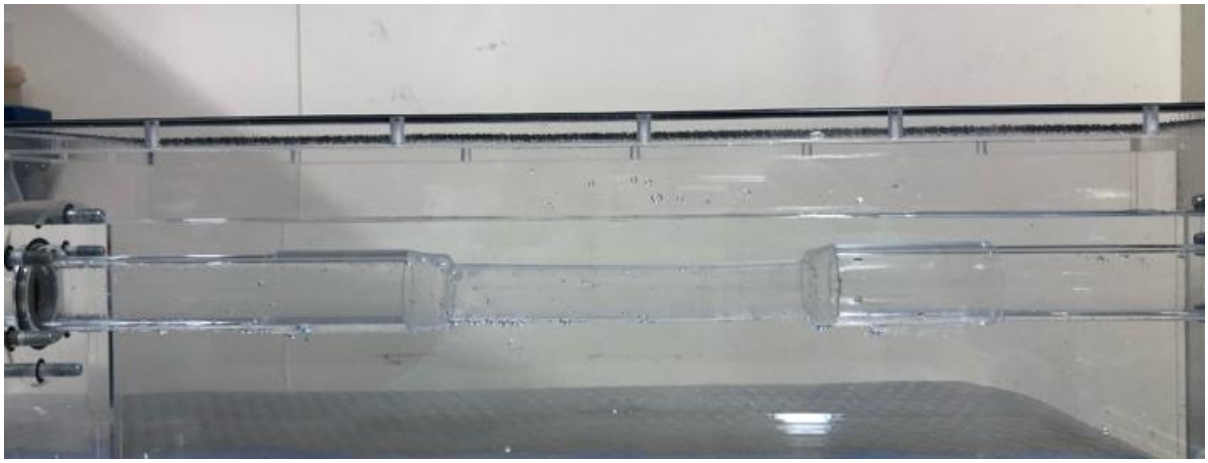

Figure 38: IVC model attached to acrylic pipes within water pressurized chamber in clean water.

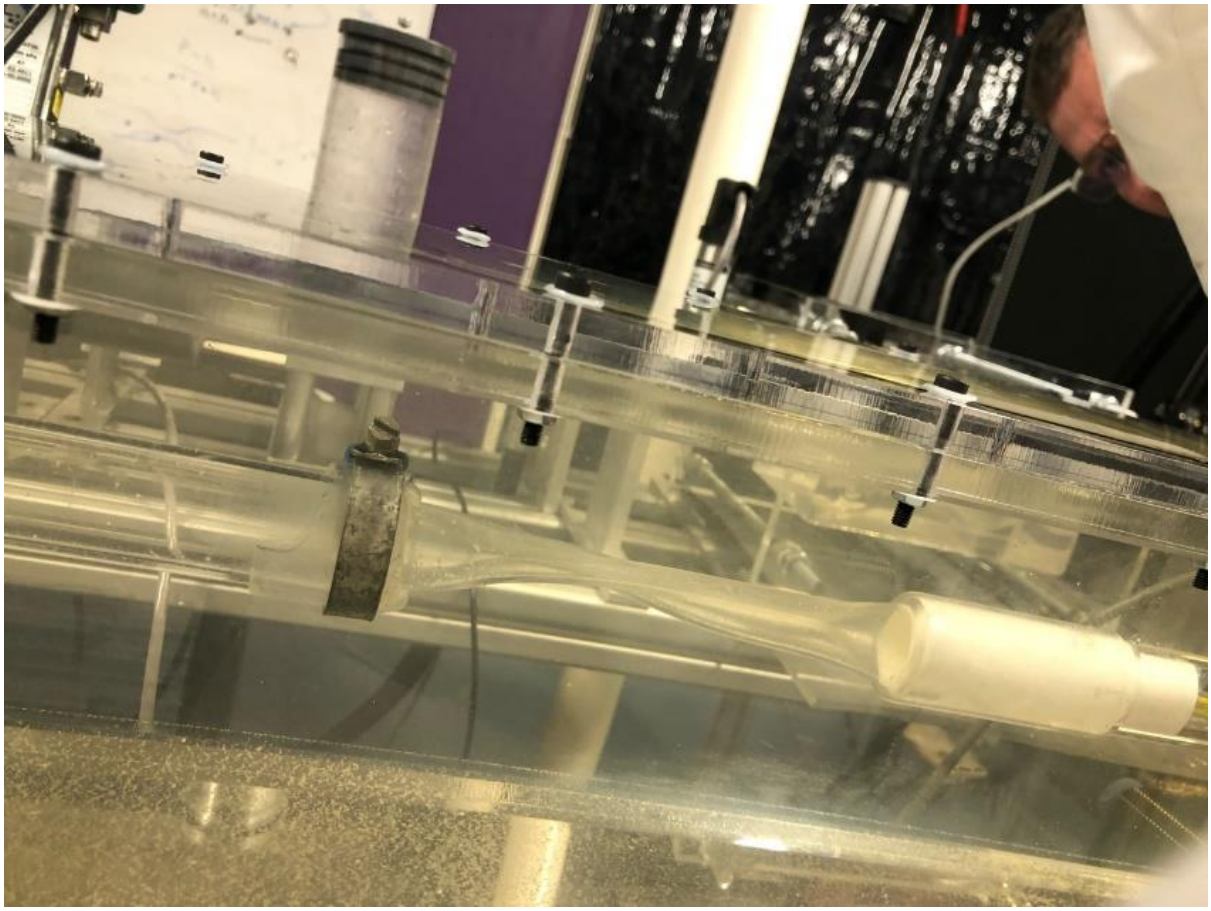

Figure 39: Model partially collapsed with BMF in pressurized chamber with added tracing particles for PIV analysis.

4.4 PIV Analysis

4.4.1 No Collapse Flow Visualization

Figures 41 and 42 are resulting images taken from the camera used for the PIV Analysis in 2 second time intervals. Figure 41 is a post-processed image of the tracking vectors of the glass particles used to visualize the flow through the model. Figures 43 and 42 compare the fluid flow through the model at low and higher flowrates.

Image 44 shows the side-view of the model, in vitro, attached to the right heart simulator by a water pressurized chamber.

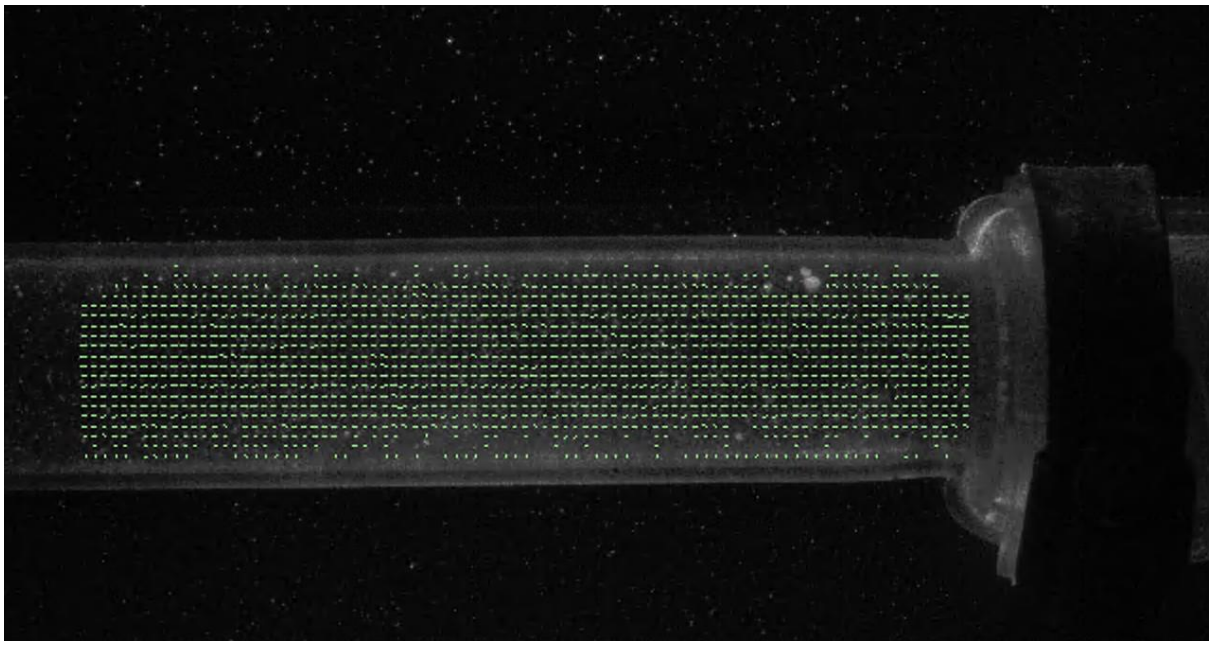

Figure 40: Non-collapsed model under steady flow conditions (20ml/s, laminar flow) Flow from right to left

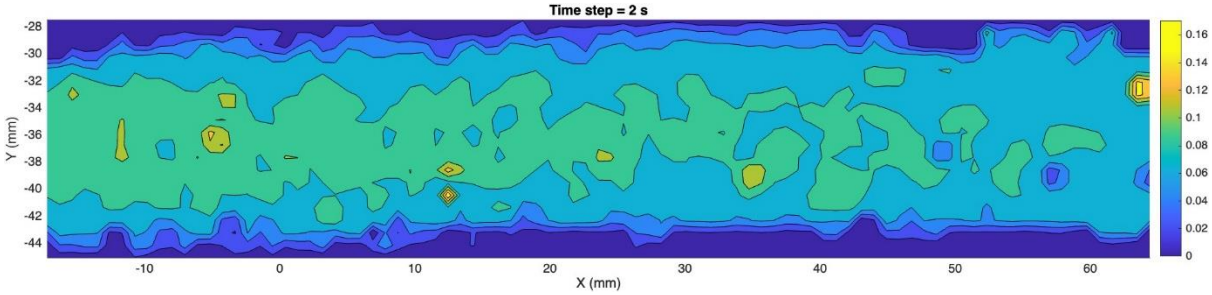

Figure 41: Laminar flow through a non-collapsed model (20 ml/s, laminar flow) showing flow along length X and across cross section Y (mm) and velocities (m/s)

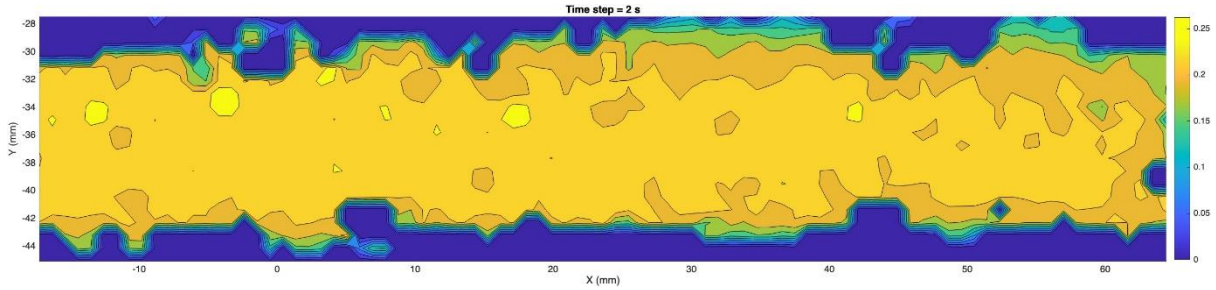

Figure 43: Turbulent flow through non-collapsed model, showing flow along length X and across cross section Y (mm) and velocities (m/s)

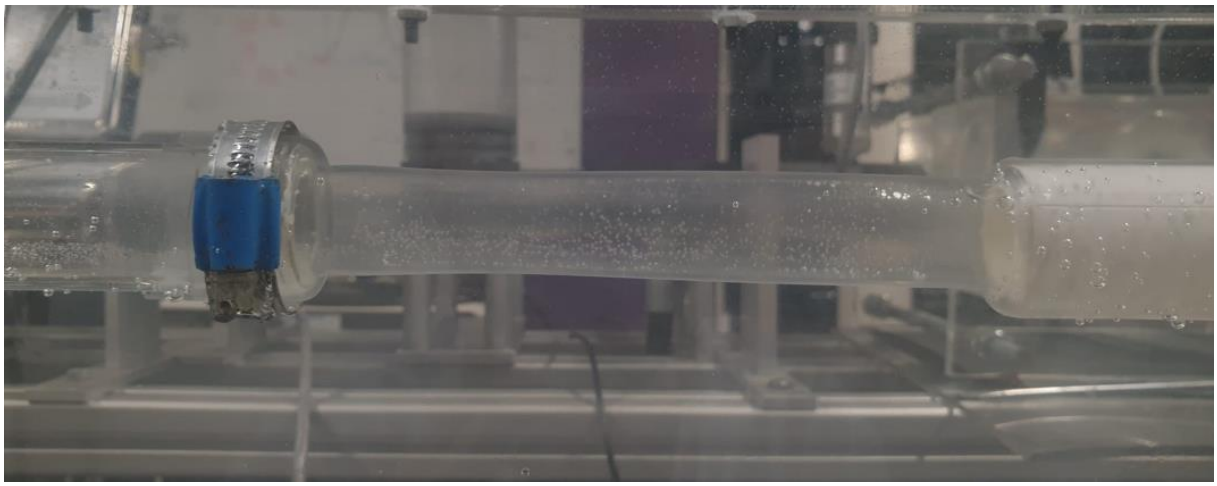

Figure 42: Non collapsed IVC model in water pressurized chamber. Flow from left to right.

4.4.2 Partially Collapsed Model Flow Visualization

Figures 45 and 46 are shown from the post-processed PIV images taken of the 100 C model, partially collapsed as shown in Figure 46. Figure 4 shows the vector fields produced by the images taken using PIV techniques.

Figure 47 shows the side-view of the model in the right heart simulator attached to a water pressurized chamber, with partial collapse applied.

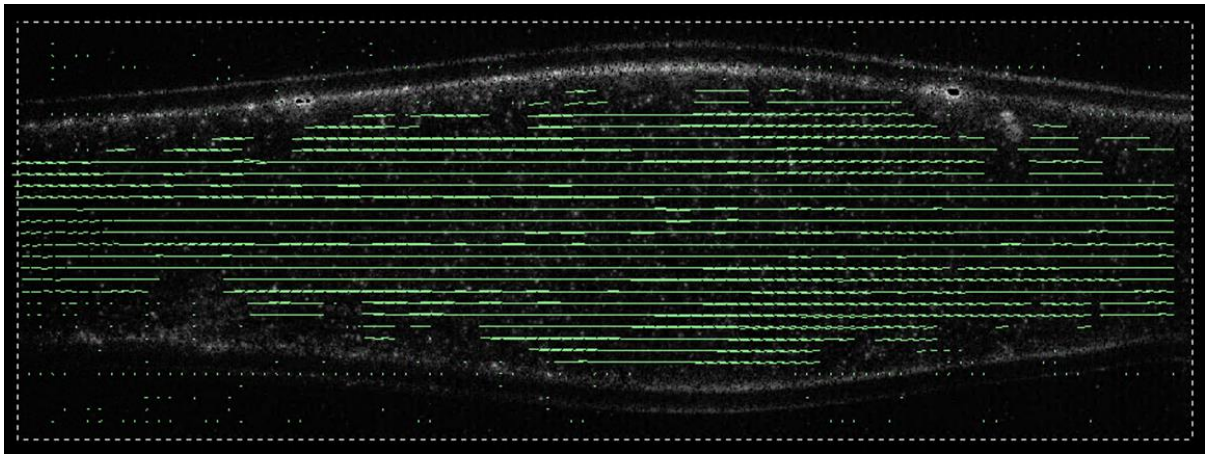

Figure 45: Collapsed vessel vector field post processed PIV images over 2 second time intervals. Flow from right to left.

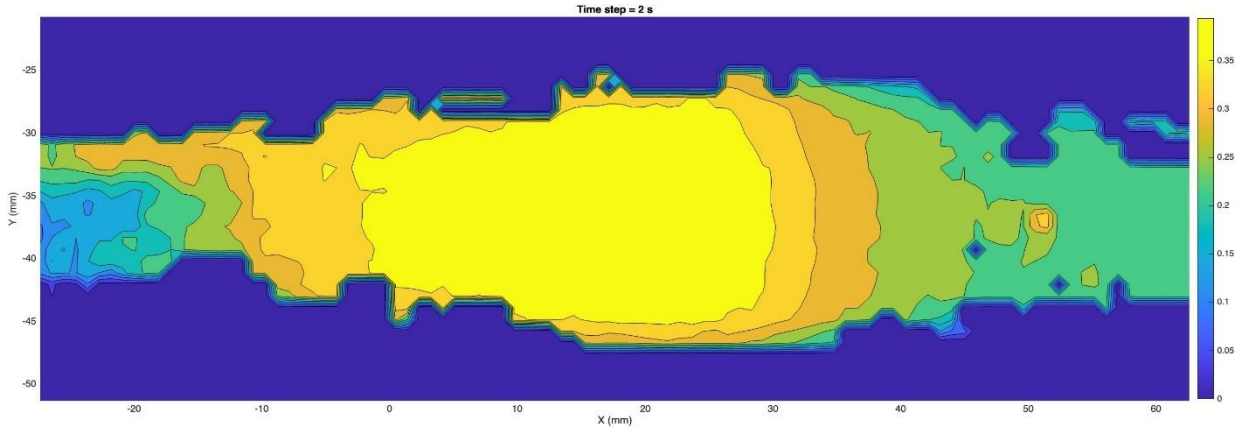

Figure 44: Flow visualization from post-processing of PIV images of a partially collapsed model. Flow is from right to left.

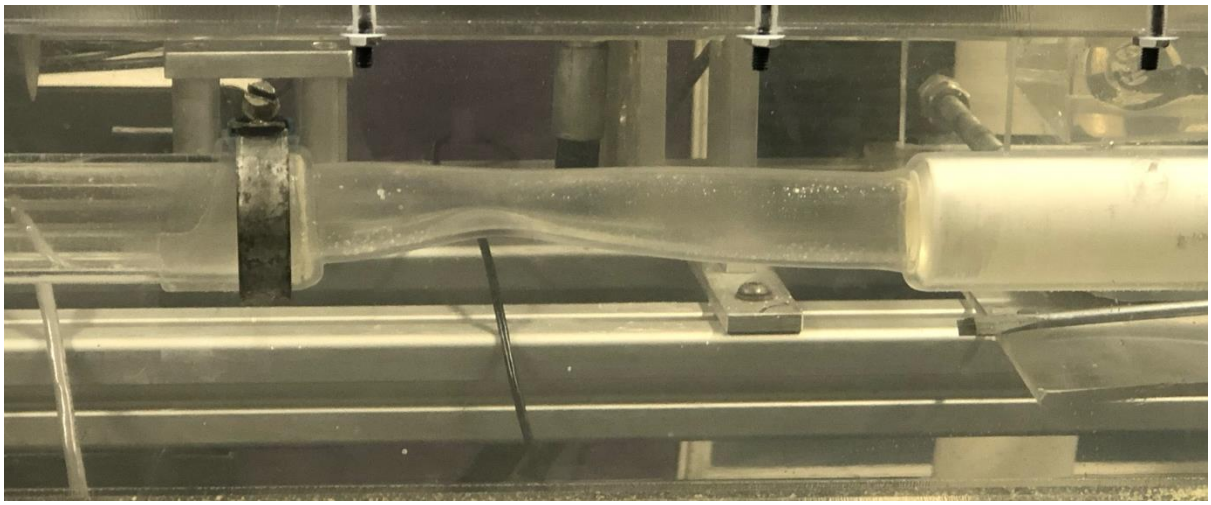

Figure 46: Partially Collapsed Model for PIV Analysis in water pressurized chamber. Flow from left to right.

4.5 Uniaxial Tensile Cyclical Testing

Sylgard-184 rings of 1.5 mm in thickness were produced, alongside the final models mentioned in Section 4.2. The methodology for designing these experiments, preparing, and conducting the testing are mentioned in Section 3.3.2. The stress-strain curves of the Sylgard-184 cured at room temperature and 100 C, give a high-level insight into the behavior of the material and the changes in behavior with the processing temperature used. Uniaxial testing is sufficient for this project, although it is recommended that circumferential testing would give a more detailed evaluation of the behavior of the material in the flow loop testing rig.

4.5.1 Uniaxial Tensile Testing: Comparison of <40% strain cyclical testing for different curing temperatures

The data shown in Figure 48 is an average of over two sample rings of Sylgard-184 for two curing temperatures (21C and 100C) subject to uniaxial tensile testing at a strain rate of 1.5 mm/min.

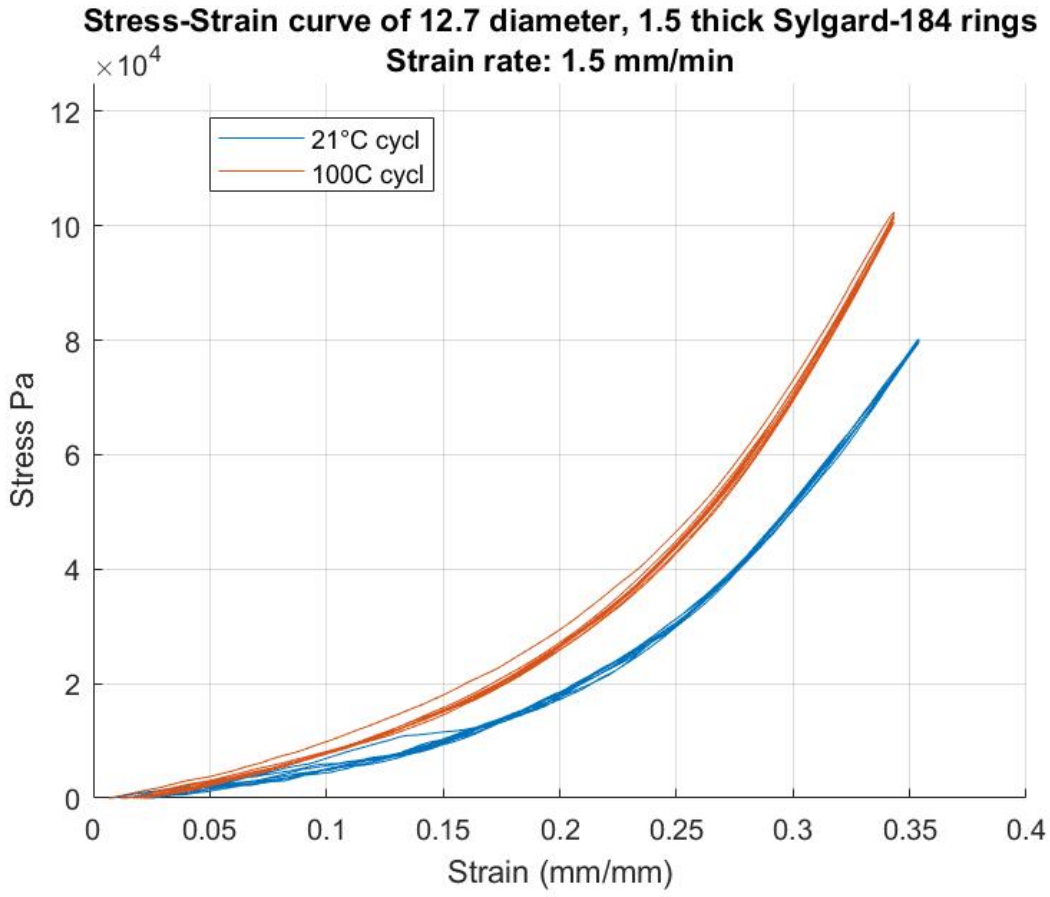

Figure 47: Comparison of cyclical mechanical strength of Sylgard-184 rings cured at 100 C and 21 C as per Dow Corning instructions. Rings were cycled 4 times and strain to approximately 35% as recommended by the literature.

4.5.2 Successive Cycling until break of 100 °C cured Sylgard-184 rings

The data illustrated in Figure 49 illustrates the stress-strain curves of Sylgard-184 subjected to 4 cycles of tensile testing at 55% and 75%. This testing was conducted at 1.5 mm/min.

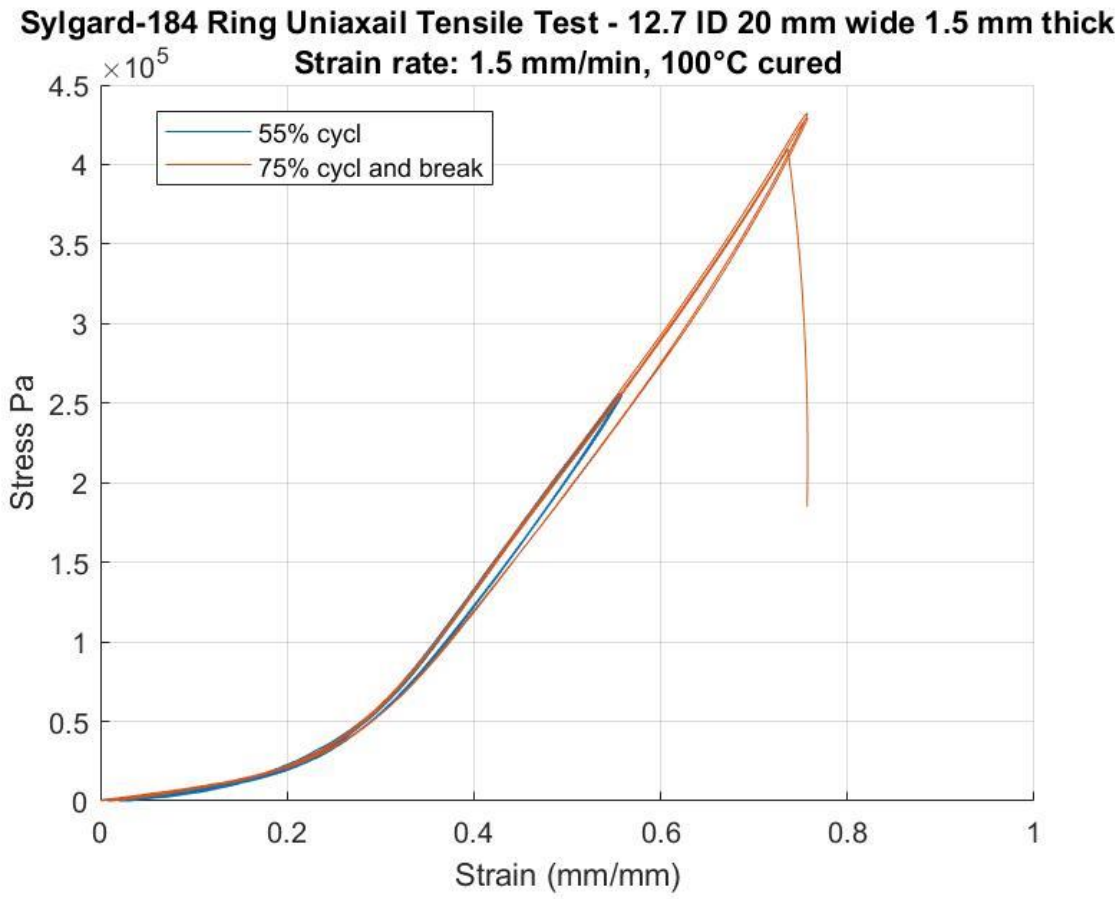

Figure 48: Comparing stress strain of Sylgard-184 to high strains of 55% and 75% with 4 cycles at each strain. Strain rate was 1.5 mm/min. Samples cured at 100 C.

4.5.3 Elastic Modulus at Low Strain Rate of Sylgard-184 cured at 100C and 21C.

The Elastic Modulus was determined by utilizing the samples previously loaded for 4 cycles, and pulling them to failure. This result gives a better idea of the mechanical strength of the materials after continous loading and unloading. The Elastic Moduli given in Table 2 are for low strain rates of less than 10%.

Table 2: Mechanical Properties obtained from Sylgard-184 after cyclical testing (4 cycles <40% strain)

Sylgard-184 Post Cyclical Testing Mechanical Properties				
Curing Temperature	**Curing Time**	**Average Low Strain Elastic Modulus (MPa)**	**Standard Deviation (MPa)**	**% Elongation at Break**
21 °C	48 hours	0.61	0.002	70.30
100 °C	1 hour	0.81	0.129	98.44

4.6 Non-standard Investigatory Tensile Tests

4.6.1 Prototype 2: Pull to Failure Test

To gain further understanding of the axial strength of the model, as Section 4.5. focuses mainly on the circumferential mechanical properties using ring samples, this section describes the nonstandard testing done with defective samples. Prototype 2 shown in Figure 36, along with a pull to failure test at 1.5 mm/min of model.

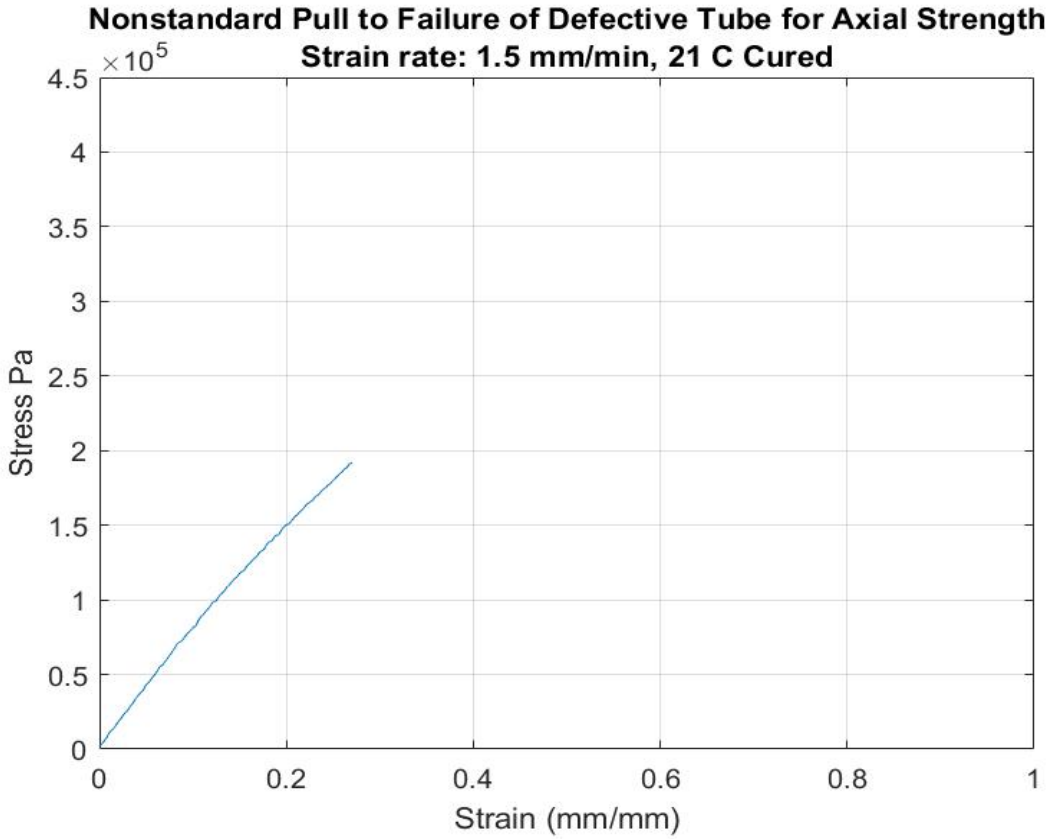

Figure 49: Prototype 2 pull to failure testing set-up for nonstandard testing. Strain rate 1.5 mm/min

4.2.7 Prototype 1: Pull to Failure Test

Figures 30 and 31 show the testing set-up for a simple pull to failure at 1.5 mm/min to understand the ultimate tensile strength, axially. Prototype 1 is clamped and pulled to failure and the resulting data is shown in Figure 34.

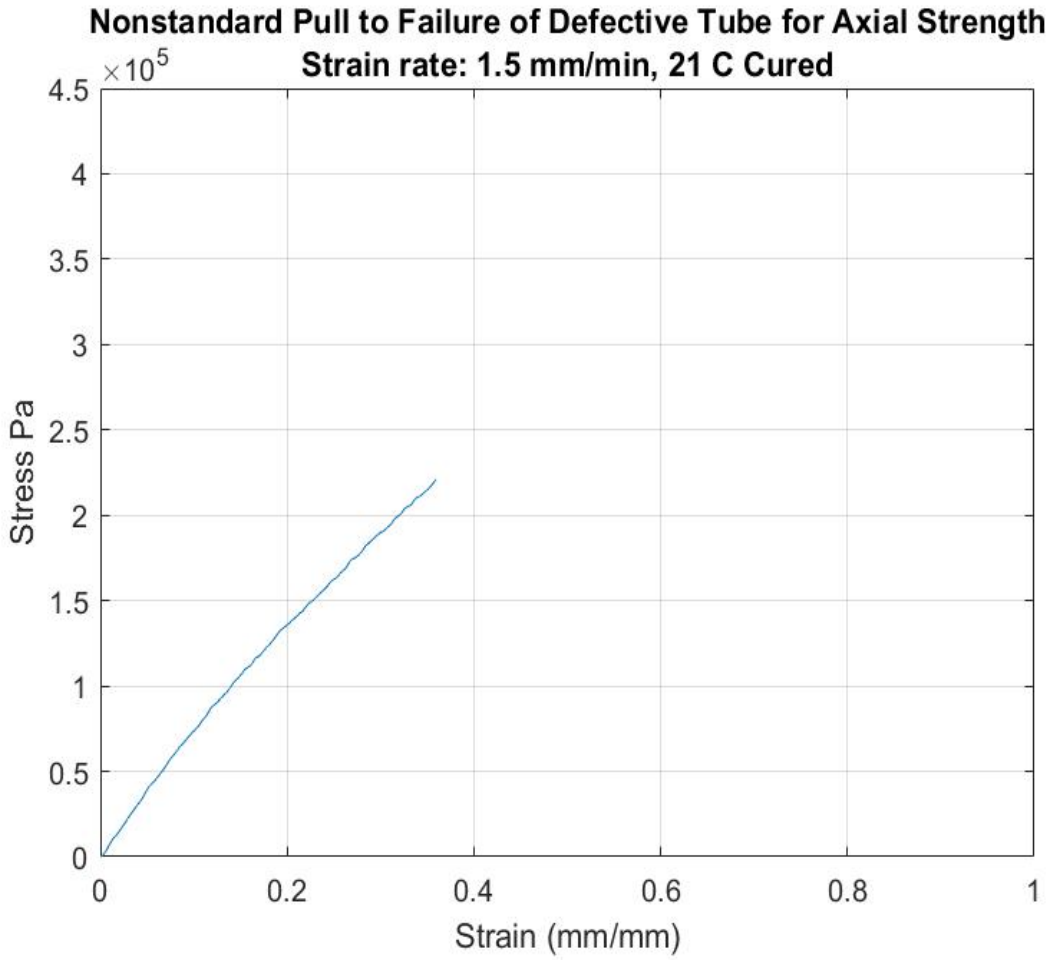

Figure 50:Prototype 1: Stress-strain relationship to show the strength of defective models for investigatory reasons. Strain rate: 1.5 mm/min.

5. Discussion

5.1 Molding and Mold Design

5.1.1 Prototypes

Sylgard-184 is a very complex material due to the tunable mechanical properties by altering processing of the material such as curing time, mixing ratio, and curing temperatures. For this project, a repeatable and standard mold design was obtained and required to ensure that the

project could be continued and used to develop further models and investigate the further effects of these properties.

Each prototype showed learnings and helped advance the design and development of both the sample ring molds and the model mold design.

Prototype 1 and 2 Learnings:

- Clingfilm not airtight enough to contain Sylgard-184 between PLA molds. Using Caulk Sealant on the edges of the molds is sufficient to contain the material.
- Horizontal curing may result in a partial model due to leakage and alternative methodology should be considered.
- Additional time for degassing is recommended and curing in a vacuum oven would be an additional measure to prevent air bubbles. The degassing time was increased from 30 minutes to 45 minutes.
- From prototype 1; adding reservoirs as seen in Figure 24, will feed excess material into the cavity if shrinkage occurs and prevent the intake of air into the mold.
- Additional clamping force was applied using a vice along with additional clamps at either end.
- Dow Corning suggests a 24-hour period for curing at room temperature, this time is doubled for ensuring the material is fully cured. Prototype 2 was left for 48 + hours to ensure the material was fully cured.
- Injection Molding the material while the mold is vertical is more efficient in pushing air out of the mold and preventing the entrapment of air bubbles.
- Mandrel splitting location and its effect on the section of the model that is required for PIV Analysis.

Using the resources available, as mentioned in Section 3.3.3 for mold design, the use of methods such as sanding, epoxy coating and mold release waxes were used to try improving the surface finish of the PLA external molds to ensure the mold release would attach to a semi-smooth surface.

Due to the shape of the mold, the epoxy resin EL2 was too fluid, and ended up accumulating in the corners of the mold and preventing the insertion of the mandrel. Miracle Gloss (Mold Release Wax) was used and did not have the effect desired, of filling in the gaps of the PLA.

The molding wax introduced a further temperature restriction with was undesirable as a solution.

Mixing epoxy resin with fillers was another attempted solution, the viscosity of the resin was increased to prevent the accumulation of the resin into the gaps. This worked the best out of the solutions although was inconsistent and resulted in non-uniformity regarding the

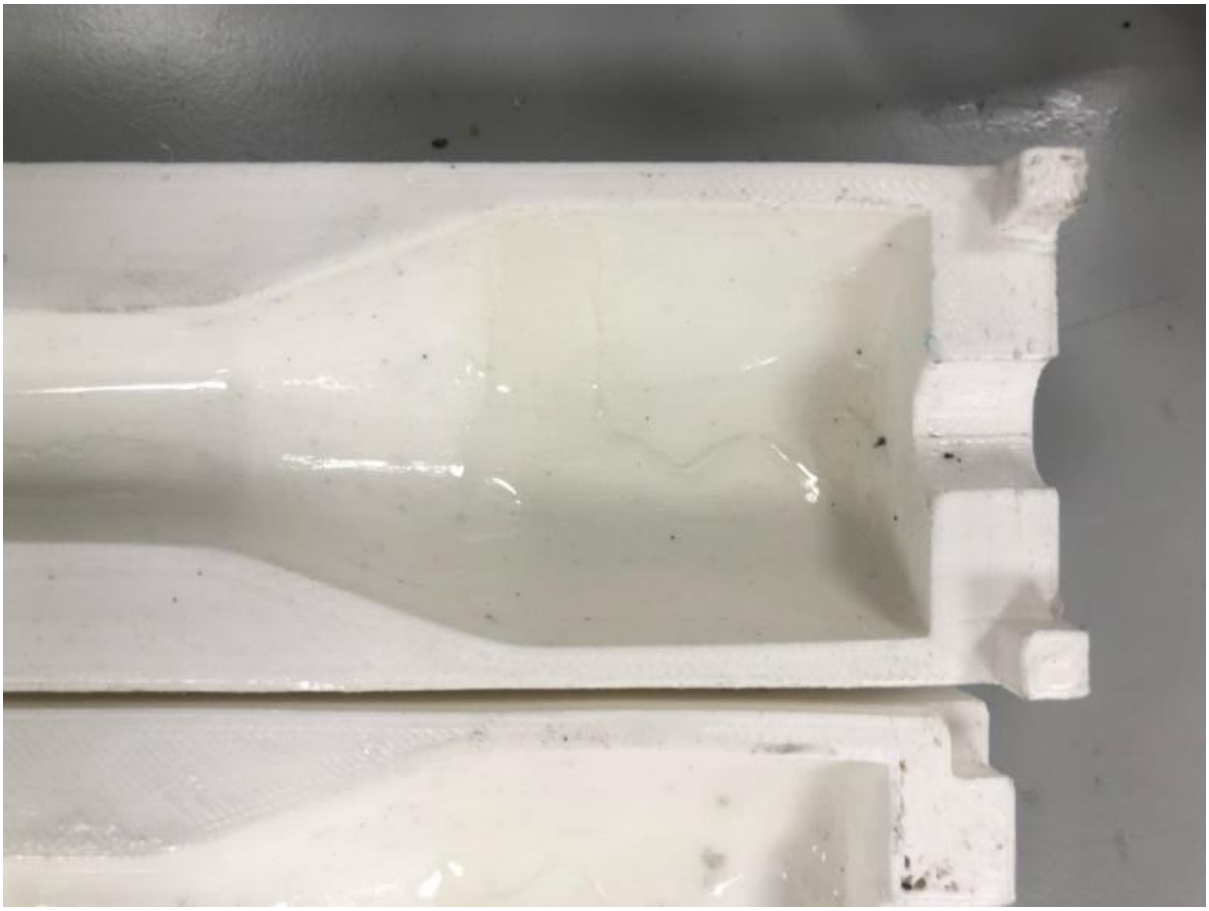

Figure 51: Resulting accumulation of epoxy resin in corners of mould due to curved surface.

5.1.2 Final Mold and Models

A new mold was designed out of Aluminum to minimize the problems with releasing the model as mentioned in Section 5.2.1.

Advantages of Aluminum Mold Design: (Figure 26.)

- A broader range of curing temperatures permitted.

- Only mold release is required for preparation of the mold. Making the process more repeatable and reliable.
- Scale of mold can be much larger due to the limited resources for additive manufacturing available without creating additional external molds.
- Ease of clamping and ensuring equal clamping pressure for full length of mold.
- Surface finish of aluminum is incomparable to sanded/epoxy-coated PLA, which allows for uninterrupted PIV Analysis.
- Cleaning of aluminum between molds is easier and there is less risk involved with cured Sylgard-184 in gaps/corners.
- Less waste with regards to materials and the use of sealant.
- The re-designed mandrel resulted in no seamline at the center of the model. Instead, the mandrel splits at one of the rig attachments on the model.

Resulting Models:

- Both models were of high transparency as shown in Figures 37 and 38. The cloudiness of the prototypes made using PLA molds of lower surface finish can be compared and this transparency can be assumed to be due to the higher surface finish of the aluminum mold surface.
- Models removed from mandrel efficiently using Isopropyl alcohol between the aluminum and elastomer.
- Model cured at lower temperature had significantly lower tear resistance and was altered to prevent tearing of the model when attaching and detaching from the chamber.
- 3D Printed attachments worked sufficiently to attach the models without flow disturbance using chamfers and gradual reduction in diameter from the inlet and outlet acrylic pipes.
- A jubilee clip is used to clamp one side of a model which has been successful in attaching the model without excessive force. Cutting the end attachment sections of the model in half is suggested for the next design to increase the ease of attachment to the acrylic tubing.

- Introduction of the material into the mold was done by attaching a luer-locking attachment and 3D Printing an elastic plug for the upper mold. This was a very repeatable process with the correct adaptor and allowed for the use of one-way valves to remove the syringe and prevent the material from exiting through the plug. This is shown below in Figures 55 and 56.

Figure 53: Plug glued to aluminium mould that allows for insertion of syringe with luer-locking adaptor. Inlet site for Sylgard-184 introduction.

Figure 52: One way valve attached to injection site to prevent leakage of material when syringe removed.

Limitations with current design:

- The reduction in size from the syringe to the plug hole shown in Figure 55 requires a large amount of force and may result in uneven pressure and insufficient packing pressure to ensure the removal of all air bubbles. Increasing the diameter for introducing the material into the mold cavity would be beneficial. A caulk gun was used to standardize the speed at which the syringe was injecting material into the mold which was effortless and worked well.
- The placement of the riser/reservoir was about 10 mm from the edge of the internal cavity end. This was a poor feature for design as it resulted in a large amount of Sylgard-184 attached at the end of the model and made it visually defective. It also resulted in a corner of the model having trapped air which was very difficult to remove and introduced tear initiation sites for the final model.
- Easier locking mechanisms for the introduction of the syringe would improve the repeatability. The current set-up using a 3D printed elastic plug for the luer adaptor is

a temporary solution. The new model in Appendix A has a threaded hole for a purchased attachment to insert into the mold. This attachment will allow for the syringe to lock onto the mold.

5.2 Cyclical Testing

The aim for the cyclical testing done was to quantify the behavior of the model used in the right heart simulator, compare to the mechanical properties of IVC tissue in the literature [12, 35] and begin to establish a testing procedure for future work with Sylgard-184 as a material. Recommendations are given in Sections 5.2.1, 5.2.2 and 5.2.3 for the procedures involved with cyclical testing of viscoelastic materials.

5.2.1 Comparison of viscoelastic hysteresis loop for 4 cycles to 35% strain for 100 C and 21 C cured rings.

Figure 48 shows the stress-strain relationship for both 21 C and 100C cured rings of Sylgard-184. Both curves show viscoelastic properties with a change in loading path after the first cycle. This is more evident for the 100 C cured sample. As expected, 100 C cured Sylgard-184 sample is stiffer with a higher stress required to strain the material to approximately 35% strain.

Additionally, the material shows the viscoelastic hysteresis loop which relates the mechanical properties of human cardiovascular tissue which is a positive outcome. Although, the loops are not very distinguishable. Additional tests would be required to see if that is strain rate dependent. Using such a low strain rate was to allow for the material to adjust since it has such a spontaneous tearing mechanism.

This loading and unloading is a preconditioning technique that is used to obtain a steady, repeatable mechanical response from the viscoelastic material [36], the resting time between loading cycles can affect the results of the material's behavior. No rest time was taken between cycles but for the continuation of testing of Sylgard-184's properties, it is recommended to ensure a standard 'preconditioned state' of the material before testing its UTS and Elastic Modulus.

It would be useful to test with a larger sample size to understand the recurrence of fracture at certain locations of the rings. This testing was not don't on a large scale but merely as an investigation to approximate the limits of the material and provide approximates for FSI simulations.

Additionally, testing at a higher strain rate would be more useful to mimic the speed of inflation and collapse that occurs *in vivo* and *in vitro* in the simulator.

5.2.2 Successive Cycling until break of 100 °C cured Sylgard-184.

From Figure 49, it was shown that the material was able to take over 50% strain for 4 cycles but failed to complete the 4 cycles over a successive 75% strain. The material fractures at about 70% strain, on the third cycle.

A lower elastic strain is shown in both curves, before the inflection point at about 30% strain, and a much stiffer, higher elastic strain is seen with a less established deflection point. Comparing to the IVC living tissue, this lower strain modulus is suggested to be dominated by behavior of elastic fibers and the higher strain modulus is suggested to be dominated by collagen fibers, all in a parallel network in the tissue [35].

It must be noted that the uniaxial method of testing is not fully representative of the actual forces that are applied to the material in the right heart simulator as force is only applied in one direction and not circumferentially.

A larger hysteresis loop is seen comparing to the previous testing done, shown in Figure 48, where the material is only stretched to under 40% strain. Comparing to the testing done on DragonSkin FX-Pro by Oisin Byrne (2021) in Figure 57, the hysteresis loops are much more distinguishable comparing to Figure 49 for Sylgard-184, and this can be due to the higher strain's reached with this more compliant material and a higher strain rate used.

DragonSkin FX-Pro shows to be almost 100 times more flexible with an ultimate tensile strength just below 1000% strain shown in Figure 57 [33]. This can be compared with Sylgard-184's fragile nature breaking below 100% strain shown in Table 2. Therefore Sylgard-184 is less compliant than DragonSkin FX-Pro and has a lower Ultimate Tensile Strength.

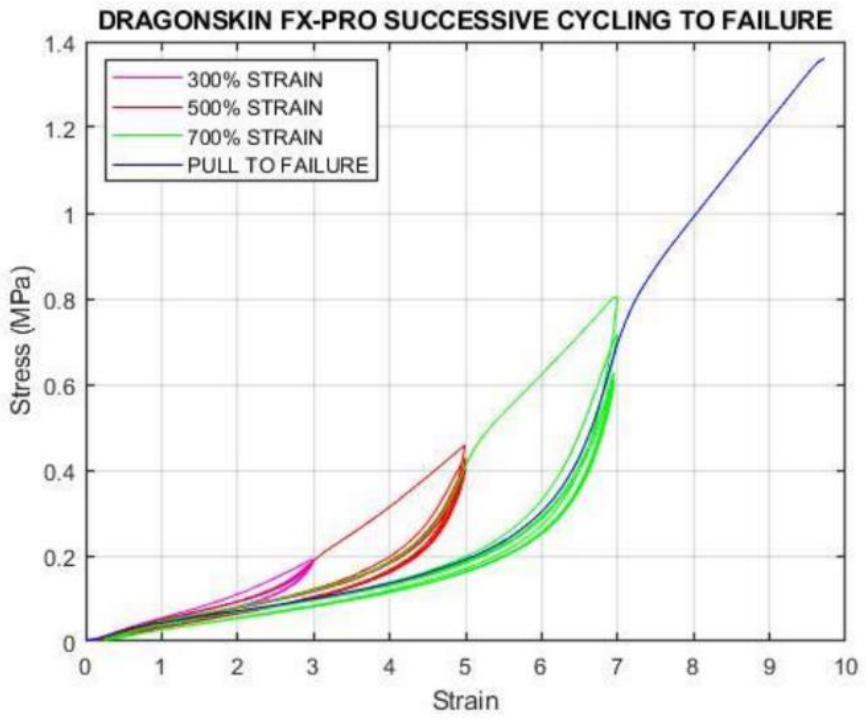

Figure 54:Comparing stress-strain curve of Dragon Skin FX-Pro subject to five cycles of cyclic uniaxial tensile testing to increasing fixed magnitude of applied strain of 300%, 500%, 700% strain then pulled to failure at a rate of 1.0 mm/s [33], (Oisin Byrne 2021)

5.2.3 Low Strain Elastic Modulus of Sylgard-184 cured at 100C and 21C.

The low elastic modulus was obtained for strain under 20% as shown in Figure 48, similarly done in the study done by Snowhill and Silver (2005) [12], on porcine tissue.

Obtaining the Young's Modulus was an objective of this test. Although the literature obtains the Young's Modulus utilizing models such as Maxwell Model for viscoelastic materials. Intuitively, the Young's Modulus was estimated by utilizing the stress-strain curves after cyclical loading when the samples were pulled to failure. This provided a value that represents the mechanical properties after it is subject to cyclical loading and unloading.

A higher modulus is seen for 100 C cured Sylgard-184 which is expected as the literature has reviewed [5] [29], therefore the model cured at the higher temperature of 100 C will have stiffer mechanical properties.

A higher elongation at break is observed for the 100 C cured Sylgard-184 which corresponds to a mechanically stronger model due to the higher modulus and higher elongation at break. This was observed in the removal of models from the mandrel since the 100 C model stayed intact with the 21 C model tearing upon removal.

5.3 PIV Analysis

The goal of this project is to utilize PIV Analysis to understand the effects of collapse of the IVC on the haemodynamics within the vessel. The Sylgard-184 model was successful in allowing for the lasers to penetrate through the material and provide a laser sheet to allow for the tracking of the seeding particles.

In Figures 44 and 47, it is shown that micro-bubbles are within the model which slight interference with the model's flow and particle tracking. Possible solutions to this problem are the following-

- Reduce the splashing/velocity of mixture entering the tank as this may be introducing the bubbles into the glycerol-water mixture and causing this issue.
- Allow for settling time after producing this mixture to allow for the bubbles to rise to the surface.
- Addition of surfactant to reduce the surface tension and prevent the formation of bubbles. Although this must be carefully done to prevent the changing of the viscosity and refractive index of the mixture.

5.3.1 No collapse

Steady flow was obtained, and flow was tracked as shown in Figure 42, using the seeding particles and two images taken within 2 seconds of each other.

Ensuring the laser sheet is in-line with the centreline of the model is important to prevent glare of the laser which may end up damaging the camera. The flow is slowest at the edges of the model due to the no-slip condition the sides of the model. The highest flow speed is shown to be approximately 0.16 m/s along the centreline, shown in Figure 41. Flow is close to 0 m/s on the edges shown in a dark blue colour in Figure 42.

Adjusting the flow into the mode, to create turbulent flow shown in Figure 43, the flow is fasters reaching 0.25 m/s for a large fraction of the volume in the model examined.

It is noted that in Figure 44, there are microbubbles attached to the internal surface of the model being analysed. This may interfere with the tracking process in PIV.

5.3.2 Partial Collapse

Figures 45 and 46 show the top-down view from the camera, of the vessels horizontal collapse upon a negative transmural pressure with relation to the abdominal chamber. The centre of the collapse experiences the highest velocities which relates the decrease in area for the fluid to flow through, accelerating the flow through the model's reduced cross section.

Figure 47 shows the side-view of the collapsed model in the simulator showing the collapse occurring closer to the upstream of the vessel. Understanding why the vessel collapses at this location rather than the downstream of the vessel is the next steps for this analysis.

Due to the model being more than twice as stiff as venous tissue [12], the pressures required to collapse the vessel are doubled which is not representative. Using the less-stiff model (cured at 21 C would bring the testing conditions closer to the *in vivo* pressure cycles.

5.4 Nonstandard Testing

The two Pull to Failure tests were done on previous prototypes (Prototype 1 and 2) labelled as defective due to a partial molded model and a model with bubbles and tears. It is worthwhile investigating the extension these models can be brought to, even with these defects, for further understanding of the material and limits.

The model in the right heart simulator currently is not yet tested with any axial strain. These tests provide a safe limit for these models to be strained if axial testing is introduced to understand its effect on the collapse location of the model in the simulator.

From these tests, a consistent result of under 40% strain of the defective models was found for the 150 mm middle section of the model. It can be concluded that a model with defects can be tested at strains lower than 40% and not fracture.

It is also noted that these tests were not cyclical. This was to test it as it would be tested in the simulator without repeated loading and unloading which the model experiences circumferentially, not axially.

This elongation at break can be compared with the 100% elongation at break of Sylgard-184 provided by Park et al (2018), [5]. This reduction in the elongation at break can be assumed to be due to the bubble formations and deformations of the models that have made them defective.

6. Conclusions and Future Work

Cardiovascular tissue's mechanical behaviors depend on their location within the vascular tree of the body and whether it is transporting oxygen to or from the heart [35]. The IVC is complex, and it has unique mechanical behaviors. This project has begun the process of manipulating PDMS elastomer, Sylgard-184, to best mimic this tissue's behaviors.

6.1 Conclusions

All the overlying aims of this project were met, a compliant, transparent model of the IVC was produced and placed in the right heart simulator.

Two models were produced to a high standard for use in the right heart simulator and for testing. These models differ in mechanical properties to demonstrate the effect of changing the curing time of the elastomer to suit its application, in this case, venous tissue of the IVC.

From the outlined aims in Section 1.2, Sylgard-184 allows for successful PIV Analysis with a refractive index matching 60-40 Water-Glycerol mixture as outlined in Section 4.3 and in the study. The models were less compliant than the previous material, DragonSkin-FX Pro used in the right heart simulator previously. Sylgard-184 shows to be a lot stiffer than DragonSkin-Pro and venous tissue itself. The low strain moduli of approximately 0.81 MPa (100C cured model) can be compared to the porcine tissue studied, with a low strain elastic moduli of 0.38 MPa [12]. This Sylgard-184 model has double the low-strain elastic modulus compared to porcine tissue. The model cured at a lower temperature has a low strain elastic modulus closer to the values obtained from Snowhill and Silver's study (2003).

For one material to be able to mimic a complicated multi-layered tissue such as IVC tissue is a very difficult (near impossible) task. Sylgard-184 is an excellent material for moving from rigid models to compliant models. It allows for the investigation into how flow is affected by the pressures upstream of vessels which will be of use to cardiovascular device companies working in this space.

Further testing is required of Sylgard-184 to obtain more accurate results to boundary conditions for FSI Simulations. Its mechanical properties have been seen to be very dependent on the processing procedure which can differ from manufacture. The material has very delicate properties which makes it difficult to manufacture and maintain.

6.2 Limitations

The limitations of this project are summarized below:

- PIV Analysis limits the material selection for the IVC model to only transparent models to ensure the laser sheet is not refracted and for easier refractive index matching. Majority of PIV analysis studies done have utilized Sylagrd-184 due to these optical properties.
- The limitations of size for additive manufacturing were noted previously. Due to the size of the model in the right heart simulator, the model had limited options with one FDM printer in the UCD Mechanical Laboratory or else a machined mold. Outsourcing was not investigated for manufacturing these molds, which would be a consideration for the project if continued.
- For testing of Sylgard-184, a biaxial machine was not in the scope of the project and testing was a secondary focus. It would be prudent to investigate circumferential and biaxial testing. The low-profile testing machine was sufficient for preliminary results regarding the mechanical properties of the material.
- The final mold design is hindered by the limitations of designing for manufacturability. These include no sharp corners in the mold's inner surface, depth of the mold, available material for use and
- The final mold design is hindered by the limitations of designing for manufacturability. These include no sharp corners in the mold's inner surface, depth of the mold, available material for use and manufacturing time.

6.3 Future Work

Section 6.3.1 will discuss the improvements that can be made to the current mold designs, possible future materials that can be used and methods that should be adapted. Section 6.3.2 discusses the recommendations for future testing methods for Sylgard-184 and procedure design.

6.3.1 Mold Design and Materials

Due to the limitations of time, investigating the effect of increasing the polymer base to curing agent ratio would be interesting and it may result in a more robust and compliant model, more suitable for IVC testing.

I believe that Sylgard-184 has potential for further mechanical tuning to improve the compliance of the material while also improving its tear resistance. Due to the primary goal of this project, producing a model using injection molding methods, only preliminary testing was done. See Section 6.3.2 for suggested testing for further understanding of the material.

Another material of interest is Elastosil M 4600 by Wacker, or one of its alternatives. It has been for visual flow measurements and could be a possible transparent alternative to Sylgard-184. It is cheaper with a lower curing time and is more robust. Although it is like DragonSkin FX-Pro as it is overly compliant with an elongation at break of 800%. One solution for this would be to mimic the multi-material approach and utilize a sleeve over this model that would produce the stiffening of the vessel at a certain diameter, like the stiffening of the IVC at higher pressures. The challenge is ensuring that this additional layer does not affect the laser's penetration and refractive index matching of the materials.

Located in Appendix A is the "next generation" of the current model mold design. It was found that certain features would reduce certain problems such as trapping of air in the mold and the ease of attaching the syringe to the mold. Moving from Aluminum which is a short-term option for designing the mold for repeatability and ensuring ease of manufacture, it would be recommended to use a harder metal such as H14 Tool Hardened Steel to prevent the scratching of the model and to improve the surface finish of the model further. The aluminum mold is soft and therefore easy to scratch which results in optical distortion for PIV Analysis.

Further research into the lost-core method should be done when developing the geometry of the IVC to include the branches off the vessel for better understanding of flow interaction of these vessels. One of the key issues with the tearing of Sylgard-184 is the removal of the mandrel from within. Using the lost-core method to mitigate this issue could be the solution, as shown in the study done by Yazdi *et al.* (2019) [34].

Ideally, this model will be used to help test the interaction of IVC diagnostic devices and the IVC environment, and it is in the future scope of this project, as the right heart simulator develops further to replicate the complex anatomies of the IVC.

6.3.2 Testing

Due to testing being a secondary aim, which was done at the tail end of this project, several changes would be made to the procedure and further developments to variables to be investigated.

The following tests are recommended to be carried out and they are recommended if Sylgard-184 is used for further model developments.

- Examining the effect of reducing ring thickness on the strength and compliance of Sylgard-184 rings. An objective would be to find the critical thickness for the model to minimize the risk of tearing when removing from mandrel and attaching to the rig.
- Examining the effect of increasing the polymer base to curing agent ratio for increased compliance. The literature has shown an increase in compliance for a higher polymer base to curing agent ratio.
- Comparing successive strains at different curing temperatures. To understand if temperature influences the overall strength when subjected to increased strain.

For cyclical testing, I would recommend using a much higher strain rate, to mimic the speed of loading and unloading in the right heart simulator. The strain rate used was kept constant, upon analysis, it would be more beneficial to be higher such as 1.5 mm/s.

For understanding the requirements for a material mimicking such a complex tissue it is important to understand the difference between the low strain elastic modulus, high strain elastic modulus and the reasons behind these mechanical behaviors such as the interaction of elastic and collagen fibers as shown in the study by Silver *et al.* 2003 [35]. I would recommend designing a standard preconditioning, that has been used in the literature for living tissue, this would make the data more comparable with the living tissue behaviors for analysis.

Due to limitations of time and processing of Sylgard-184, inflation tests were not done for this project to measure the static compliance of the material. It would be advised to test tubes of

different thicknesses, curing temperatures and mixing ratios to tune the mechanical properties to lower the stiffness of the material, for bio-fidelity.

6.4 Sustainability

Simulated use systems are increasingly being used in the medical device sector to improve sustainability. These systems provide a way to test medical devices in a controlled environment that replicates real-world use conditions. This enables manufacturers to identify potential issues and make design improvements before the product is released to market, reducing waste, and improving the overall sustainability of the medical device sector.

The three UN Sustainable Development Goals that are very relevant to the goals of this project are the following: Goal 3, Goal 9, and Goal 12.

Figure 57: UN Sustainability Goal 3

Figure 56: UN Sustainability Goal 12

Figure 55: UN Sustainability Goal 9

Goal 3: Good Health and Well-Being.

The advancement of research into vascular anatomies allows one to understand the effects of disease on the body. Certain diagnostic devices are being developed for heart failure detection using the Inferior Vena Cava. This project aids towards the larger goals of faster diagnosis of heart disease, reducing the number of deaths related to heart disease, reducing hospital bills for heart transplants and risky surgeries and an overall increase in the general health of all populations worldwide. Diagnostics and digital health are relatively new areas in the medical device sector and will lead to a more equitable healthcare system.

Goal 9: Industry, Innovation, and Infrastructure

This Sustainability goal calls for the development of sustainable and resilient infrastructure and the promotion of inclusive and sustainable industrialization. By promoting sustainable manufacturing practices in the medical device sector, simulated use systems contribute to the achievement of this goal.

Simulated-use testing systems make innovation more accessible to organizations that do not have the funding to invest in multiple animal studies to understand the human body's response to their new technology. This will accelerate the growth of the start-up culture for medical devices in Ireland who compete with the MedTech giants such as Medtronic and Stryker.

Goal 12: Responsible Consumption and Production

The overarching goal of this project is to understand the flow of the human body using imaging techniques and to eventually test devices, measuring their effect on flow. Simulated-use systems can reduce the amount of waste in the manufacturing process of medical devices by pinpointing problems in the early stages of design, while also reducing the cost of re-designing the product. Simulated-use systems promote more responsible consumption and production practices.

Utilizing the data obtained from the PIV analysis done on the model, the computer simulations can be improved using flow rates, mechanical properties and other values obtained from testing. The improvement of these FSI simulations results in more robust online testing, further reducing plastic and other material waste in the re-designing stages of devices.

6.5 Ethics

The project touches on many ethical areas including inclusivity of medical device design and reducing the number of animal studies done for device validation for approval. Medical devices are often designed and tested using data primarily collected from non-minority populations which leads to ineffective and often harmful devices for minority populations. The lack of participation and stringent eligibility criteria in clinical trials results in problematic and dangerous medical device designs for these populations [37].

Simulated-use systems allow for device testing in vitro and allow for adaptability of the testing for each human anatomy. This improves the safety of medical devices by testing the fit and response of devices in replicas of human anatomies taken from CT scans. This project contributed to the future in the medical device testing of the IVC and understanding the response of the IVC to respiration and cardiac cycles.

Throughout the validation and verification stages of medical device processes, many animal studies are opted for to understand how the device reacts to irregularities in anatomy, physiology, and environment. This is expensive, unethical, and time-consuming. The development of robust haptic simulators mimicking human physiology will reduce the need for animal studies. A MIT laboratory developed a bionic heart that is used to test prosthetic hearts, which Dr Roche states will “reduce the amount of animal testing”, in the MIT News Article [2].

This project will hopefully in the future reduce the need for animal testing of IVC devices throughout the device validation and verification stages of product development. Not only does this make this process more ethical but it reduces costs for medical device companies, speeds up design development stages and helps to identify device failure modes early in the development process.

Figure 58: 3D Printed bionic custom heart made in MIT Laboratory for heart valve testing [2].

7. Bibliography

[1] Y. C. Fung, *Biomechanics : Circulation*. New York, NY, UNITED STATES: Springer New York, 1996.

[2] J. Chu, "Engineers design bionic “heart” for testing prosthetic valves, other cardiac devices," in *MIT News*, ed: MIT News Office, 2020.

[3] D. Seliktar, R. A. Black, R. P. Vito, and R. M. Nerem, "Dynamic Mechanical Conditioning of Collagen-Gel Blood Vessel Constructs Induces Remodeling In Vitro," *Annals of Biomedical Engineering,* vol. 28, pp. 351-362, 2000. Annals of Biomedical Engineering.

[4] P. I. Aaronson, J. P. T. Ward, and M. J. Connolly, *The Cardiovascular System at a Glance*. Hoboken, UNITED KINGDOM: John Wiley & Sons, Incorporated, 2012.

[5] S. Park *et al.*, "Silicones for Stretchable and Durable Soft Devices: Beyond Sylgard-184," *ACS Applied Materials & Interfaces,* vol. 10, no. 13, pp. 11261-11268, 2018/04/04 2018, doi: 10.1021/acsami.7b18394. ACS Applied Materials & Interfaces.

[6] H. Nisar, J. Moore, R. Piazza, E. Maneas, E. C. S. Chen, and T. M. Peters, "A simple, realistic walled phantom for intravascular and intracardiac applications," *International Journal of Computer Assisted Radiology and Surgery,* vol. 15, no. 9, pp. 1513-1523, 2020/09/01 2020, doi: 10.1007/s11548-020-02201-3. International Journal of Computer Assisted Radiology and Surgery.

[7] P. Hajikarimi and F. Moghadas Nejad, "Chapter 3 - Mechanical models of viscoelasticity," in *Applications of Viscoelasticity*: Elsevier, 2021, pp. 27-61. Applications of Viscoelasticity.

[8] C. P. Cheng, "Chapter 12 - Inferior Vena Cava and Lower Extremity Veins," in *Handbook of Vascular Motion*: Academic Press, 2019, pp. 247-271. Handbook of Vascular Motion.

[9] H. J. Smith, P. Grøttum, and S. Simonsen, "Ultrasonic assessment of abdominal venous return. II. Volume blood flow in the inferior vena cava and portal vein," (in eng), *Acta Radiol Diagn (Stockh),* vol. 27, no. 1, pp. 23-7, Jan-Feb 1986, doi: 10.1177/028418518602700105. Acta Radiol Diagn (Stockh).

[10] M. Y. Yousif, D. W. Holdsworth, and T. L. Poepping, "Deriving a blood-mimicking fluid for particle image velocimetry in Sylgard-184 vascular models," (in eng), *Annu Int Conf IEEE Eng Med Biol Soc,* vol. 2009, pp. 1412-5, 2009, doi: 10.1109/iembs.2009.5334175. Annu Int Conf IEEE Eng Med Biol Soc.

[11] D. B. Camasão and D. Mantovani, "The mechanical characterization of blood vessels and their substitutes in the continuous quest for physiological-relevant performances. A critical review," (in eng), *Mater Today Bio,* vol. 10, p. 100106, Mar 2021, doi: 10.1016/j.mtbio.2021.100106. Mater Today Bio.

[12] P. B. Snowhill and F. H. Silver, "A Mechanical Model of Porcine Vascular Tissues-Part II: Stress–Strain and Mechanical Properties of Juvenile Porcine Blood Vessels," *Cardiovascular Engineering,* vol. 5, no. 4, pp. 157-169, 2005/12/01 2005, doi: 10.1007/s10558-005-9070-1. Cardiovascular Engineering.

[13] R. K. Brawley, H. N. Oldham, J. S. Vasko, R. P. Henney, and A. G. Morrow, "Influence of right atrial pressure pulse on instantaneous vena caval blood flow," (in eng), *Am J Physiol,* vol. 211, no. 2, pp. 347-53, Aug 1966, doi: 10.1152/ajplegacy.1966.211.2.347. Am J Physiol.

[14] L. Wexler, D. H. Bergel, I. T. Gabe, G. S. Makin, and C. J. Mills, "Velocity of blood flow in normal human venae cavae," (in eng), *Circ Res,* vol. 23, no. 3, pp. 349-59, Sep 1968, doi: 10.1161/01.res.23.3.349. Circ Res.

[15] A. J. Narracott, "The Venous System," in *Cardiovascular Biomechanics*. Cham: Springer International Publishing, 2017, pp. 127-142. Cardiovascular Biomechanics.

[16] F. L. L. Moreno, A. D. Hagan, J. R. Holmen, T. A. Pryor, R. D. Strickland, and C. H. Castle, "Evaluation of size and dynamics of the inferior vena cava as an index of right-sided cardiac function," *The American Journal of Cardiology*, vol. 53, no. 4, pp. 579-585, 1984/02/01/ 1984, doi: https://doi.org/10.1016/0002-9149(84)90034-1. The American Journal of Cardiology.

[17] T. C. Gasser, *Vascular Biomechanics: Concepts, Models, and Applications*. Stockhold Sweeden: Springer, 2022.

[18] B. P. Brown and D. D. Heistad, "Capacitance of the rabbit portal vein and inferior vena cava," (in eng), *J Physiol*, vol. 381, pp. 417-25, Dec 1986, doi: 10.1113/jphysiol.1986.sp016335. J Physiol.

[19] Z. Wang, M. J. Golob, and N. C. Chesler, "Viscoelastic Properties of Cardiovascular Tissues," 2016.

[20] S. P. Glasser *et al.*, "Vascular compliance and cardiovascular disease: a risk factor or a marker?," (in eng), *Am J Hypertens*, vol. 10, no. 10 Pt 1, pp. 1175-89, Oct 1997, doi: 10.1016/s0895-7061(97)00311-7. Am J Hypertens.

[21] G. Biglino, P. Verschueren, R. Zegels, A. M. Taylor, and S. Schievano, "Rapid prototyping compliant arterial phantoms for in-vitro studies and device testing," *Journal of Cardiovascular Magnetic Resonance*, vol. 15, no. 1, p. 2, 2013/01/16 2013, doi: 10.1186/1532-429X-15-2. Journal of Cardiovascular Magnetic Resonance.

[22] S. Kefayati and T. L. Poepping, "3-D flow characterization and shear stress in a stenosed carotid artery bifurcation model using stereoscopic PIV technique," in *2010 Annual International Conference of the IEEE Engineering in Medicine and Biology*, 31 Aug.-4 Sept. 2010 2010, pp. 3386-3389, doi: 10.1109/IEMBS.2010.5627933.

[23] R. Lindken and S. Burgmann, "14 - Laser-optical methods for transport studies in low temperature fuel cells," in *Polymer Electrolyte Membrane and Direct Methanol Fuel Cell Technology*, vol. 2: Woodhead Publishing, 2012, pp. 425-461. Polymer Electrolyte Membrane and Direct Methanol Fuel Cell Technology.

[24] S. Zhang, C. Ge, and R. Liu, "Mechanical characterization of the stress-strain behavior of the polydimethylsiloxane (PDMS) substate of wearable strain sensors under uniaxial loading conditions," *Sensors and Actuators A: Physical*, vol. 341, p. 113580, 2022/07/01/ 2022, doi: https://doi.org/10.1016/j.sna.2022.113580. Sensors and Actuators A: Physical.

[25] P. H. Geoghegan, N. A. Buchmann, C. J. T. Spence, S. Moore, and M. Jermy, "Fabrication of rigid and flexible refractive-index-matched flow phantoms for flow visualisation and optical flow measurements," *Experiments in Fluids*, vol. 52, no. 5, pp. 1331-1347, 2012/05/01 2012, doi: 10.1007/s00348-011-1258-0. Experiments in Fluids.

[26] C. J. T. Spence, N. A. Buchmann, M. C. Jermy, and S. M. Moore, "Stereoscopic PIV measurements of flow in the nasal cavity with high flow therapy," *Experiments in Fluids*, vol. 50, no. 4, pp. 1005-1017, 2011/04/01 2011, doi: 10.1007/s00348-010-0984-z. Experiments in Fluids.

[27] L. M. Hopkins, J. T. Kelly, A. S. Wexler, and A. K. Prasad, "Particle image velocimetry measurements in complex geometries," *Experiments in Fluids*, vol. 29, no. 1, pp. 91-95, 2000/07/01 2000, doi: 10.1007/s003480050430. Experiments in Fluids.

[28] K. Khanafer, A. Duprey, M. Schlicht, and R. Berguer, "Effects of strain rate, mixing ratio, and stress-strain definition on the mechanical behavior of the polydimethylsiloxane (PDMS) material as related to its biological applications," (in English), *Biomedical Microdevices*, vol. 11, no. 2, pp. 503-8, Apr 2009

2014-08-30 2009, doi: https://doi.org/10.1007/s10544-008-9256-6. Biomedical Microdevices.

[29] I. D. Johnston, D. K. McCluskey, C. K. L. Tan, and M. C. Tracey, "Mechanical characterization of bulk Sylgard 184 for microfluidics and microengineering," *Journal of Micromechanics and Microengineering*, vol. 24, no. 3, p. 035017, 2014/02/28 2014, doi: 10.1088/0960-1317/24/3/035017. Journal of Micromechanics and Microengineering.

[30] Y.-C. Fung, "Mechanical Properties and Active Remodeling of Blood Vessels," in *Biomechanics: Mechanical Properties of Living Tissues*. New York, NY: Springer New York, 1993, pp. 321-391. Biomechanics: Mechanical Properties of Living Tissues.

[31] Y. C. Fung, "Bio-viscoelastic Solids," in *Biomechanics: Mechanical Properties of Living Tissues*. New York, NY: Springer New York, 1981, pp. 196-260. Biomechanics: Mechanical Properties of Living Tissues.

[32] A. Colombo, H. Zahedmanesh, D. M. Toner, P. A. Cahill, and C. Lally, "A method to develop mock arteries suitable for cell seeding and in-vitro cell culture experiments," *Journal of the Mechanical Behavior of Biomedical Materials*, vol. 3, no. 6, pp. 470-477, 2010/08/01/ 2010, doi: https://doi.org/10.1016/j.jmbbm.2010.04.003. Journal of the Mechanical Behavior of Biomedical Materials.

[33] O. Byrne, "Further compliance testing of silicone phantoms with emphasis on recreating inferior vena cava compliance in vitro," University College Dublin, Thesis, 2021.

[34] S. G. Yazdi *et al.*, "A Novel Fabrication Method for Compliant Silicone Phantoms of Arterial Geometry for Use in Particle Image Velocimetry of Haemodynamics," *Applied Sciences*, vol. 9, no. 18, p. 3811, 2019. Applied Sciences.

[35] F. H. Silver, P. B. Snowhill, and D. J. Foran, "Mechanical Behavior of Vessel Wall: A Comparative Study of Aorta, Vena Cava, and Carotid Artery," *Annals of Biomedical Engineering*, vol. 31, no. 7, pp. 793-803, 2003/07/01 2003, doi: 10.1114/1.1581287. Annals of Biomedical Engineering.

[36] G. Bianco, A. M. Levy, R. Grytz, and M. A. Fazio, "Effect of different preconditioning protocols on the viscoelastic inflation response of the posterior sclera," *Acta Biomaterialia*, vol. 128, pp. 332-345, 2021/07/01/ 2021, doi: https://doi.org/10.1016/j.actbio.2021.04.042. Acta Biomaterialia.

[37] M. Hussain-Gambles, K. Atkin, and B. Leese, "Why ethnic minority groups are under-represented in clinical trials: a review of the literature," *Health & Social Care in the Community*, vol. 12, no. 5, pp. 382-388, 2004, doi: https://doi.org/10.1111/j.1365-2524.2004.00507.x. Health & Social Care in the Community.

Appendix A: Future Work Next Gen Design

A.1: Upper External Mold

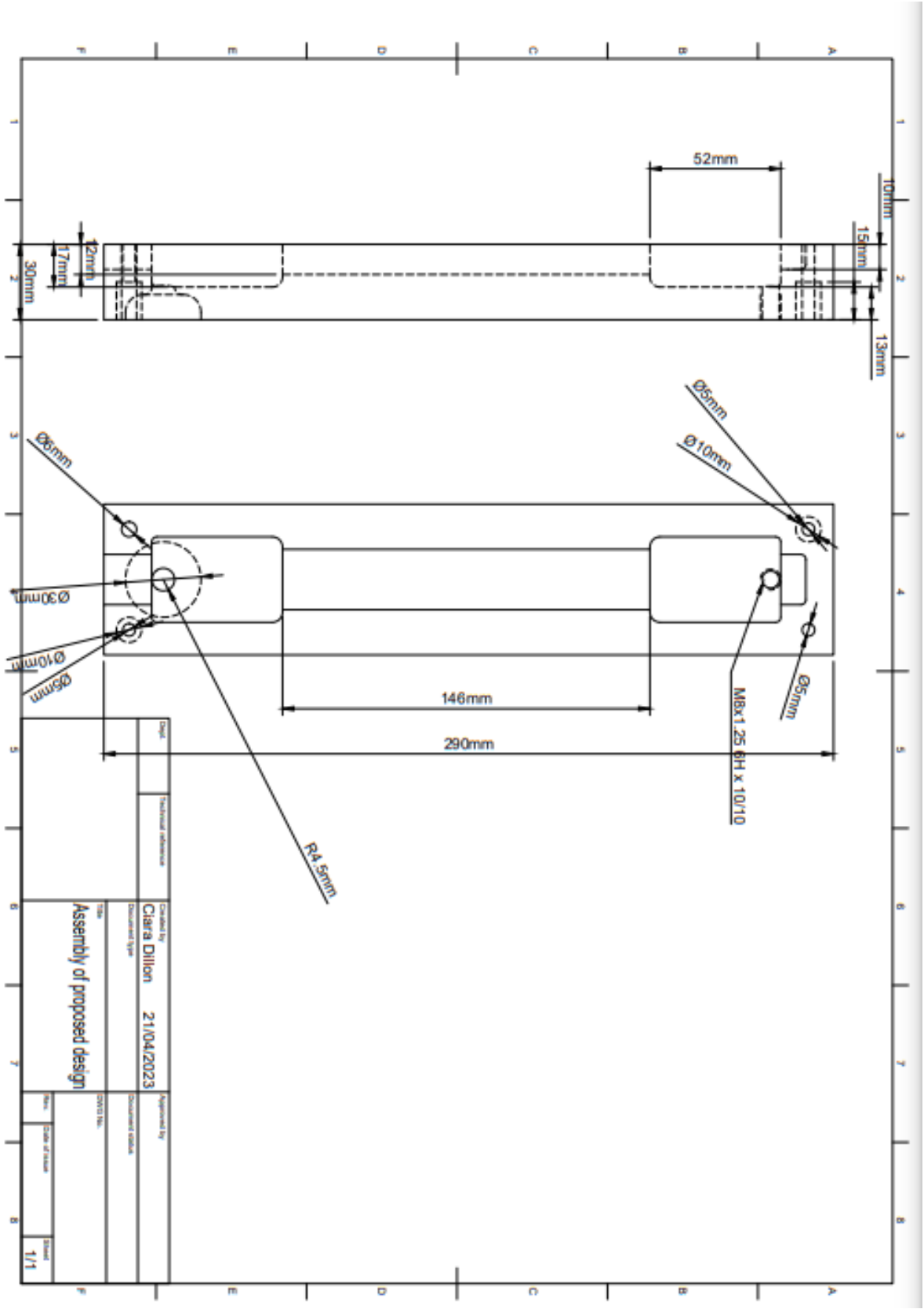

A.2 Lower External Mold (mm)

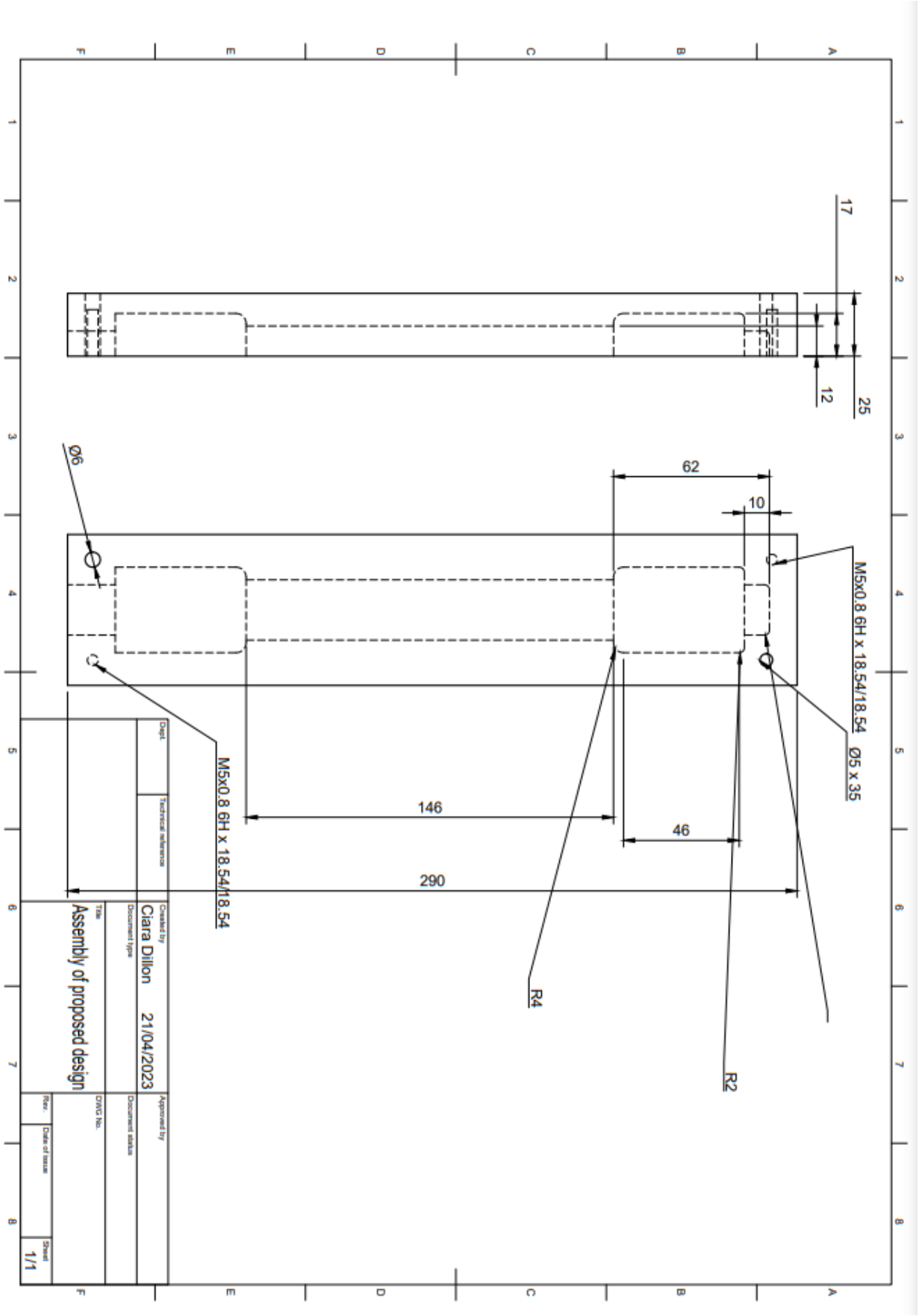

A.3 Mandrel Part 1 (mm)

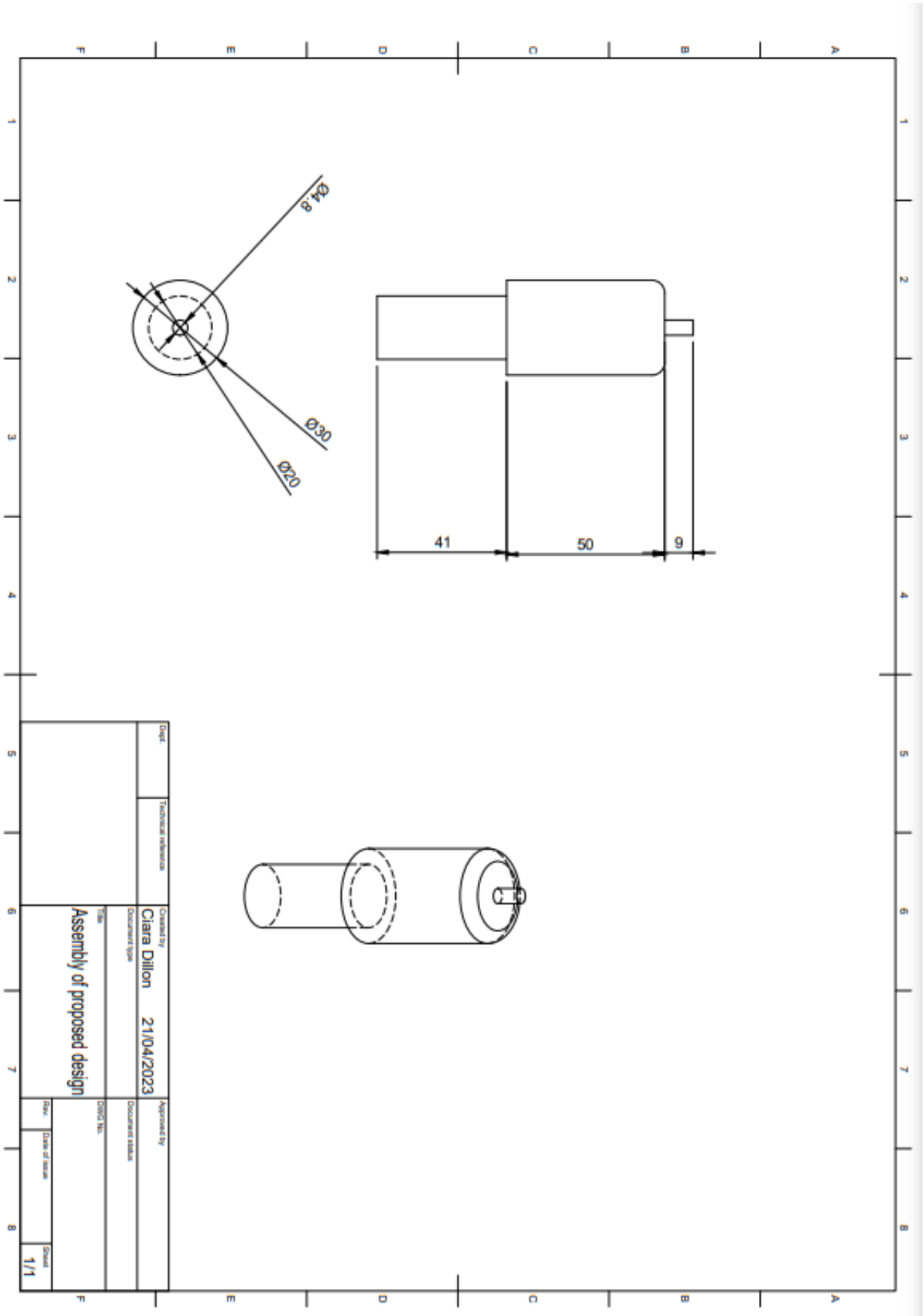

A.4 Mandrel Part 2